Topological Classes of Stationary Axisymmetric Black Holes

By

Haseeb Nazar

NATIONAL UNIVERSITY OF MODERN LANGUAGES
ISLAMABAD

July, 2025

A Topological Classes of Stationary Axisymmetric Black Holes

By

Haseeb Nazar

MS-Math, National University of Modern Languages, Islamabad, 2025

A THESIS SUBMITTED IN PARTIAL FULFILMENT OF

THE REQUIREMENTS FOR THE DEGREE OF

MASTER OF SCIENCE

In **Mathematics**

To

FACULTY OF ENGINEERING & COMPUTING

NATIONAL UNIVERSITY OF MODERN LANGUAGES ISLAMABAD

THESIS AND DEFENSE APPROVAL FORM

The undersigned certify that they have read the following thesis, examined the defense, are satisfied with overall exam performance, and recommend the thesis to the Faculty of Engineering and Computing for acceptance.

Thesis Title: Topological Classes of Stationary Axisymmetric Black Holes

Submitted By: Haseeb Nazar **Registration #:**50 MS/MATH/S22

Master of Science in Mathematics

Title of the Degree

Mathematics

Name of Discipline

Dr. Muhammad Rizwan _____

Name of Research Supervisor Signature of Research Supervisor

Dr. Sadia Riaz _____

Name of HoD (Mathematics) Signature of HoD (Math)

Dr. Noman Malik _____

Name of Dean (FEC) Signature of Dean (FEC)

July, 2025

AUTHOR'S DECLARATION

I Haseeb Nazar

Son of Nazar Hayat

Discipline Mathematics

Candidate of Master of Science in Mathematics at the National University of Modern Languages, do hereby declare that the thesis Topological Classes of Stationary Axisymmetric Black Holes submitted by me in partial fulfilment of MS degree, is my original work and has not been submitted or published earlier. I also solemnly declare that it shall not, in the future, be submitted by me for obtaining any other degree from this or any other university or institution. I also understand that if evidence of plagiarism is found in my thesis/dissertation at any stage, even after the award of a degree, the work may be canceled and the degree revoked.

Signature of Candidate

Haseeb Nazar

Name of Candidate

July 18, 2025

Date

ABSTRACT

Title: Topological Classes of Stationary Axisymmetric Black Holes

In recent years, the study of black holes has gained significant attention, particularly in the context of their topological properties. In this thesis, we investigate the topological numbers of Kiselev black holes, rotating Kiselev black holes, Kerr-Newman black holes, and Kerr-AdS black holes in the presence of a quintessential field. Our primary focus is to analyze whether the quintessential field influences the topological number of these black holes. We classify the black holes into three topological classes based on the topological: -1, 0, and 1. Through our analysis, we find that the presence of the quintessential field does not affect the topological number of these black holes. Additionally, in the case of Kerr-Ads black holes, we observe the presence of an annihilation point. To further investigate the impact of the quintessential field, we explore the effect of the state parameter ω within the interval $-1 < \omega < -1/3$ by selecting different values. Our results indicate that while the curves exhibit slight deviations, the winding number and topological number remain unchanged. Similarly, we analyze the impact of varying the quintessential parameter c and find that it does not alter the topological number of black holes. These findings suggest that the quintessential field does not play a role in modifying the topological nature of black holes. Since topological numbers are crucial in understanding black hole thermodynamics, our study provides valuable insights into the stability and classification of black holes in the presence of exotic fields..

TABLE OF CONTENTS

LIST OF TABLES

LIST OF FIGURES

LIST OF ABBREVIATIONS

EFEs	-	Einstein's Field Equations
GSL	-	Generalized Second Law of Thermodynamics
CMB	-	Cosmic Microwave Background
WIMPs	-	Weakly Interacting Massive Particles
TOV	-	Tolman–Oppenheimer–Volkoff
BH	-	Black Hole
EHT	-	Event Horizon Telescope
W	-	Winding number
GP	-	Generation Point
AP	-	Annihilation Point

LIST OF SYMBOLS

$R_{\mu\nu}$	-	Ricci Curvature Tensor
Λ	-	Cosmological Constant
G	-	Gravitational Constant
$T_{\mu\nu}$	-	Stress-Energy Tensor
M	-	Mass
Q	-	Charge
$\mathscr{F}$	-	Off-shell free energy
S	-	Entropy
τ	-	Inverse of Temperature

ACKNOWLEDGMENT

First and foremost, I would like to express my profound gratitude and sincere appreciation to Almighty Allah, whose countless blessings and guidance made this research work possible and successful.

This study could not have been accomplished without the valuable support and encouragement of many individuals. I am deeply indebted to my research supervisor, Dr. Muhammad Rizwan, whose continuous guidance, patience, and expertise were instrumental in shaping this work. His unwavering support throughout my research journey has been truly invaluable.

I would also like to extend my heartfelt gratitude to our Head of Department Dr. Sadia Riaz, whose kind support and efforts to provide a productive research environment played a significant role in the completion of this work.

My sincere thanks go to the esteemed faculty members, including , Dr. Anum Naseem, Dr. Hadia Tariq, Dr. Aisha Anjum, and other teachers for their guidance and assistance during this journey. Additionally, I greatly appreciate the efforts of the administrative staff, whose cooperation and support helped overcome many challenges during my research experience.

DEDICATION

This thesis work is dedicated to my parents, family, and my teachers throughout my education career who have not only loved me unconditionally but whose good examples have taught me to work hard for the things that I aspire to achieve.

CHAPTER 1

INTRODUCTION

1.1 General Relativity

The Newtonian theory of gravity is based on the idea of time as a universal quantity that is the same for everyone, regardless of whether they are moving or at rest. In this framework, time is independent of the observer's velocity and position in space. Thus, according to this theory, the arena of physics is 3-dimensional space. Furthermore, Newton explains gravity as a force that attracts distinct objects to each other, which is proportional to their masses and inversely proportional to the distance between them. The Newtonian theory provides a mathematical expression for calculating the gravitational force, but it does not explain why distant objects are attracted to each other. This theory best describes the motion of bodies moving at low velocities compared to the speed of light and motion in weak gravitational fields. However, it is unable to explain the bending of light due to massive gravitational objects and, particularly, the shift in Mercury's orbit.

In 1905 his theory of special relativity, Einstein proposed that time is not universal; that is, it is not the same for everyone. Instead, it depends on the observer's velocity [1, 2]. So, instead of a 3-dimensional space, he introduces the idea of spacetime, which combines space and time into a single 4-dimensional manifold called spacetime. John Wheeler summarized this as "*spacetime is the arena of physics where all events occur*" [2]. Einstein extended the framework of special relativity to include gravity, introducing the concept that gravity arises from the curvature of

spacetime caused by mass and energy. Therefore, general relativity focuses on understanding the shape and structure of spacetime using a type of geometry called pseudo-Riemannian geometry. The line element that provides the spacetime interval between two events in the special theory of relativity can be written as

$$ds^2 = -c^2dt^2 + dx^2 + dy^2 + dz^2, \tag{1.1}$$

where c represents the velocity of light and negative sign in the first term on the right-hand side is due to the signature choice $(-,+,+,+)$. The line element is an invariant quantity, equivalent to the distance measured in Euclidean space. The spacetime interval between two events can be zero, positive, or negative. The general form of the line element required to study the spacetime manifold used the pseudo-Riemannian metric and is can be expressed as [2]

$$ds^2 = g_{\mu\nu}dx^\mu dx^\nu, \tag{1.2}$$

where $\mu,\nu = 0,1,2,3$ and $g_{\mu\nu}$ represents the second-rank. Einstein's theory of general relativity relates the curvature of spacetime to the distribution of matter and energy within it through the EFEs, given as [2, 3, 4]

$$R_{\mu\nu} - \frac{1}{2}Rg_{\mu\nu} + \Lambda g_{\mu\nu} = kT_{\mu\nu}, \tag{1.3}$$

Here, $R_{\mu\nu}$ represents the Ricci curvature tensor, R denotes the Ricci scalar, Λ is the cosmological constant, and $T_{\mu\nu}$ is the stress-energy tensor representing the distribution of matter and energy in spacetime. The constant k, referred to as Einstein's constant, is defined as

$$k = \frac{8\pi G}{c^4},$$

where G is Newton's gravitational constant and c is the speed of light in vacuum. This constant determines the strength of the coupling between the geometry of spacetime and the matter-energy content within it. According to J. A. Wheeler, this theory implies a dynamic interplay between space and matter: space drives matter movement, while matter controls space curvature. In the above field equation, Einstein introduce the the cosmological constant Λ, used this constant to maintain a static universe solution, as the popular belief then was that the cosmos was unchanging, neither expanding nor contracting. The cosmological constant was designed to oppose the gravitational attraction between matter in the cosmos, creating a repulsive force that could balance the gravitational pull and keep the universe steady. It was mathematically expressed as Λ in EFEs. However, in 1929, Edwin Hubble's pioneering observations of distant

galaxies revealed that the cosmos is not static, but rather expanding. Hubble's finding, known as Hubble's Law, revealed that galaxies are moving apart, indicating that the universe is expanding. As a result of this realization that the cosmos was not static as he had first believed, Einstein was able to declare the introduction of the cosmological constant the "biggest blunder" of his career. Even though Einstein was initially skeptical, the cosmological constant has subsequently been reexamined in cosmology as a potential explanation for the universe's observed accelerated expansion, especially in light of dark energy. Therefore, EFEs without a cosmological constant can be expressed as,

$$R_{\mu\nu} - \frac{1}{2}Rg_{\mu\nu} = kT_{\mu\nu}. \tag{1.4}$$

The four dimensions of spacetime (one-time dimension and three spatial dimensions) are represented by the numbers $0, 1, 2$, and 3 for the indices μ and ν. A system of ten equations comes from each pair of indices (μ, ν) since the metric tensor $g_{\mu\nu}$is symmetric (i.e., $g_{\mu\nu} = g_{\nu\mu}$). Expanding the EFEs forms a system of ten partial differential equations. These mathematical equations clarify how matter and energy (represented by the stress-energy tensor, $T_{\mu\nu}$ affect spacetime geometry (through the metric tensor $g_{\mu\nu}$). Second derivatives of the metric tensor components are involved in these second-order equations. Due to their extreme nonlinearity, the terms include complex relationships between the derivatives and products of the metric components. The first and second derivatives both illustrate this non-linearity. Because the EFEs are linked and non-linear (each equation depends on several variables and functions), solving them directly for a generic situation is very difficult. There are certain presumptions and simplifications made to handle this complexity. Physical relevance has been suggested for matter and energy distribution (the stress-energy tensor $T_{\mu\nu}$. The equations are made simpler by making assumptions about spacetime symmetries (such as spherical symmetry or static solutions). By making assumptions about the symmetries and features of spacetime, we can reduce the number of independent variables and functions to solve. Selecting a suitable coordinate system can make the problem even simpler. A vacuum, which has no matter or energy in it, is the most straightforward scenario to think about. The stress-energy tensor $T_{\mu\nu} = 0$ in this instance. The Minkowski spacetime, which is a representation of flat, space with no curvature, is the solution with the highest symmetry in a vacuum. In Minkowski spacetime, the metric tensor has been given by $g_{\mu\nu} = diag(-1, 1, 1, 1)$, showing a flat spacetime with different time and spatial dimensions, where distances are measured as they would be in Euclidean space [2, 3, 4].

Astronomically, these objects are formed when a massive star (greater than 1 the mass of

three solar masses) collapses due to its gravitational pull at the end of its life cycle. Astronomers categorise BHS into three primary groups: intermediate-mass, supermassive, and stellar mass. A stellar-sized BH is formed when a star is at least 20 times as massive as the Sun collapses. Supermassive BHs are huge-sized black holes with a mass range from 105 to a billion solar masses. Every galaxy is believed to have a supermassive BH in its center. Recently, the Event Horizon Telescope has released images of the supermassive BH at the center of our Milky Way and the neighbouring galaxy M87 [5].

Spacetime, as described by black holes, is a fascinating and complex concept in the context of general relativity, Albert Einstein's theory of gravity. According to general relativity, space and time are interconnected into a four-dimensional fabric known as spacetime. Imagine spacetime as a massive, flexible trampoline. Normally, everything is smooth and flat, but near black holes, things become chaotic. According to physicist John Wheeler, spacetime is not constant at the smallest scale. Instead, it resembles a bubbling pot of water, constantly moving and rattling. This "foamy" character implies that spacetime is not stable but fluctuates constantly. Wheeler's idea helps us understand how space and time operate in the severe conditions around black holes when gravity's pull is powerful [2]. We'll review fundamental concepts from Newtonian and special-relativistic perspectives on space and time to understand the relativistic theory of gravity. To define an event uniquely, we must assign it three Space and time coordinates defined relative to a frame of reference. To define a system S, consider three mutually orthogonal Cartesian axes (x, y, z) and a system of synchronized clocks at rest t. The four coordinates (t, x, y, z) label time and space events. In technical terms, it constitutes a 4-dimensional manifold (M, g); essentially, a space resembling a Euclidean 4-dimensional space on a local scale.

1.2 Black Hole

The escape velocity of a gravitation body is the minimum speed required for an object to overcome the gravitational pull of body, without needing any extra thrust. It is a fundamental concept in astrodynamics and celestial mechanics, crucial for understanding space travel and the behavior of celestial objects [6]. The escape velocity of any gravitational object of mass M at a

distance r from its center of mass is defined as

$$\upsilon_{esc} = \sqrt{\frac{2GM}{r}}, \tag{1.5}$$

where G denotes the universal gravitational constant. From the definition of escape velocity, we can see that at any point P, the escape velocity of a gravitational object is directly proportional to the square root of its gravitational mass M and inversely proportional to the square root of the distance r from the center of the gravitational object. For reference, the escape velocity at the surface of Earth is $11.3km/s$, while for the Sun, it is $615km/s$.

A black hole forms when a significant amount of mass is compressed into a very small space, usually within the Schwarzschild radius. For example, if you could compress three times the mass of the Sun into a space smaller than its Schwarzschild radius, a black hole would develop. The concept of escape velocity is critical to understanding black holes. As an object's mass increases, its escape velocity also increases, meaning the gravitational pull becomes stronger, making it more difficult for anything—including light—to escape.

Classically, black holes are defined as gravitational objects with extraordinarily strong gravity, such that their escape velocities exceed the speed of light [2]. Therefore, to escape a black hole's pull, an object would need to move at a velocity greater than the speed of light, which is not possible. Consequently, nothing not even light can escape from the black hole's spacetime. As light loses its ability to escape the gravitational pull, we cannot see these objects directly; however, we can observe them by studying the behavior of neighboring stars and their environments. Initially, these objects were called dark stars and were later named black holes [7]. A spherical boundary in spacetime around the singularity, at which the escape velocity is exactly equal to the speed of light, is called an event horizon. Inside this surface, the escape velocity exceeds the speed of light, meaning that nothing can escape—not even light. Outside this surface, the escape velocity is less than the speed of light, allowing light to reach an observer at a distance far away from the central object. This boundary is known as the black hole's event horizon [8]. Matter collapses under its gravitational pull to form a black hole, and when it reaches a critical density, the escape velocity becomes greater than the speed of light.

A black hole's "information paradox" arises because any knowledge about its contents is permanently concealed beyond its event horizon. There are two types of black holes: static and rotating. The event horizon of a non-rotating black hole is spherical and stationary, while rotating black holes have two horizons. These have an oblate spheroid shape, with an inner and outer event horizon (the outer being analogous to the Schwarzschild horizon). The event horizon

itself is undetectable; therefore, gravitational lensing and Hawking radiation are used to explain observations [9, 10]

$$R_S = \frac{2GM}{c^2}. \tag{1.6}$$

In this case, G signifies Newton's gravitational constant, and c stands for the speed at which light travels in a vacuum.

1.3 Schwarzschild Black Hole

In 1916, shortly after Einstein presented his theory of general relativity, Karl Schwarzschild provided the first solution to EFEs. He considered a point gravitational source of mass M is located at the origin and else there is a vacuum everywhere. Further, he consider the spacetime to be spherically symmetric and static and obtained the solution of EFS known as the Schwarzschild spacetime solution.

The line element of a Schwarzschild black hole in spherical coordinates (in natural units, $G = 1, c = 1$) can be written as [1, 2]

$$ds^2 = -\left(1 - \frac{2M}{r}\right) dt^2 + \left(1 - \frac{2M}{r}\right)^{-1} dr^2 + r^2 d\theta^2 + r^2 \sin^2\theta d\phi^2. \tag{1.7}$$

Here ds^2 is the line element representing the distance between the two spacetime events, θ coordinate (similar to latitude) and ϕ is coordinate (similar to longitude) and M is mass of the central body, t is time coordinate r is coordinate (distance from the center). As gravity increases (higher M), these terms diverge from one, showing that spacetime is no longer flat. The metric coefficient g_{tt} is not defined at $r = 0$, the origin itself, which is the essential singularity of the spacetime where the curvature invariants are not well defined and the laws of physics break down. There is another location $r = 2M$ called the Schwarzschild radius, at this location the metric component g_{rr} is not define how ever the curvature invariants are finite, hence showing that this is not an essential singularity but it is a coordinate singularity that can be removed using a coordinate transformation. This surface is of great instead and is the event horizon of the Schwarzschild black hole, and behaves like a point of no return because inside this surface the escape velocity is greater than the speed of light, and at this surface the escape velocity is exactly equal to the speed of light.

The Schwarzschild solution is suitable for describing the gravitational field outside a spherical, non-rotating mass (for example, a star, planet, or black hole), assuming the black hole is either non-rotating or rotating slowly. If the conditions for collapse are just right, black holes of various masses may exist. The photon sphere is a region located just outside the event horizon, at $3/2$ times the Schwarzschild radius. In this region, light can theoretically travel in circular orbits; however, even a minor disruption can causes the light to either fall into the black hole or escape.

1.4 Reissner-Nordström Black Hole

Following the formulation of general relativity by Einstein in 1915 and the subsequent discovery of the Schwarzschild solution in 1916, the study of black holes expanded significantly. In this context, Hans Reissner and Gunnar Nordström independently developed the Reissner-Nordström solution, with Reissner's work in 1916 and Nordström's in 1918. This solution builds on the Schwarzschild metric by incorporating the effects of electric charge, addressing both electromagnetic and gravitational fields. Specifically, the Reissner-Nordström solution considers the influence of an electric charge q and a mass M. Outside a charged black hole, the metric describing spacetime remains static and spherically symmetric, indicating that it does not change over time. Notably, the solution satisfies both Maxwell's equations, which govern electromagnetic fields, and Einstein's field equations, which describe gravitational fields.

The line element of the Reissner-Nordstrom black hole can be written as [1, 11]

$$ds^2 = -\left(1 - \frac{2M}{r} + \frac{q^2}{r^2}\right) dt^2 + \left(1 - \frac{2M}{r} + \frac{q^2}{r^2}\right)^{-1} dr^2 + r^2 d\theta^2 + r^2 \sin^2\theta d\phi^2. \quad (1.8)$$

Here, the time component g_{tt} represents the time dilation effect due to the blak hole mass and charge. The radial component g_{rr} explains how the gravitational and electromagnetic fields increase distances in a radial direction. The angular components ($g_{\theta\theta}$ and $g_{\phi\phi}$) describe the geometry of a 2-dimensional sphere of radius r in terms of the angles θ (colatitude) and φ (longitude). The term $2M/r$ represents the gravitational potential due to the mass M of the BH. The expression q^2/r^2 describes the electrostatic potential resulting from the charge q of the spacetime. The metric reduces to the Schwarzschild solution for $q = 0$, where the BH is described as uncharged. In addition to gravitational attraction, the presence of q modifies the Schwarzschild metric by adding a repulsive electrostatic force.

Note that, unlike the Schwarzschild black hole, the Reissner-Nordström line element has two locations where the metric component g_{rr} is not well defined, referred to as the two horizons: the inner horizon (r_-) and the outer event horizon (r_+). These horizons are found by solving the horizon equation $r^2 - 2Mr + q^2 = 0$, yielding the value

$$r_\pm = M \pm \sqrt{M^2 - q^2}. \tag{1.9}$$

The above equation shows that the line element (1.8) represents the Reissner-Nordström black hole with two horizons only if $q < M$. For $M = q$, the two horizons merge to a single horizon and the line element represents an extremal black hole. However, for $M < q$ the horizon equation has no real root and the essential singularity at $r = 0$ is not covered by an event horizon and can therefore be observed by an outside observer. In this case, the element is referred to as a naked singularity, and the spacetime is not classified as a black hole.

The electromagnetic field surrounding the charged black hole is described by the vector potential A^α, which has four components. The first component of the four-potential corresponds to a purely electrostatic field (with no magnetic component) and has a potential that falls off as $1/r$. This solution illustrates how the interaction between general relativity and electromagnetism shapes the geometry of spacetime around a charged black hole.

A charged, non-rotating massive object is described by the Reissner-Nordström metric. The Schwarzschild metric, which represents an uncharged, non-rotating massive object, is obtained by setting the charge $q = 0$. Both metrics approximate the Minkowski metric, which describes flat spacetime, as the ratio $2M/r$ approaches 0. [2, 3, 4].

1.5 Kerr-Newman Black Hole

The Kerr and Kerr-Newman black holes are types of rotating black holes proposed by Roy Kerr and Ezra Newman in the early 1960s. Rotating black holes form when a massive, spinning star undergoes gravitational collapse, or when compact objects, such as stars, collide with a total angular momentum that is not zero. Since all known stars rotate and realistic collisions typically involve nonzero angular momentum, it is expected that all black holes in nature are rotating.

The Kerr black hole is characterized by two parameters: mass M and rotation a. In contrast, the Kerr-Newman black hole generalizes the Kerr solution by introducing an additional parameter:

the charge q of the black hole. This generalization was a significant advancement, providing a comprehensive description of rotating, charged black holes.

A key result in the study of general relativity is the Kerr-Newman solution, which represents the most complete description of a black hole that accounts for mass, charge, and rotation. It offers valuable insights into how black holes behave under various physical scenarios and highlights the diversity and complexity of solutions to Einstein's field equations [2, 3, 4]. The spacetime surrounding a BH is described by the three parameters of the Kerr-Newman metric is given by:

$$ds^2 = -\frac{\Delta}{\Sigma}\Big[dt - a\sin^2\theta d\phi\Big]^2 + \frac{\Sigma}{\Delta}dr^2 + \Sigma d\theta^2 + \frac{\sin^2\theta}{\Sigma}\Big[\left(r^2+a^2\right)d\phi - adt\Big]^2, \quad (1.10)$$

where

$$\Delta = r^2 - 2Mr + Q^2 + a^2 \quad and \quad \Sigma = r^2 + a^2 cos^2\theta. \quad (1.11)$$

The one-form of the electromagnetic 4-potential, which defines the electromagnetic field in spacetime, is expressed as

$$A_\mu dx^\mu = -\frac{Qr}{\Sigma}\Big(dt - asin^2\theta d\phi\Big). \quad (1.12)$$

This expression provides a description of the electromagnetic interaction in the context of spacetime geometry, incorporating the influence of the black hole's rotation.
The black hole possesses two horizons, which correspond to the real solutions of the equation.

$$r^2 - 2Mr + Q^2 + a^2 = 0, \quad (1.13)$$

and can be expressed as

$$r_\pm = M \pm \sqrt{M^2 - Q^2 - a^2} \quad \text{with} \quad a^2 + Q^2 \leq M^2. \quad (1.14)$$

If $M^2 < a^2 + Q^2$, the solutions become imaginary, and the line element (3.7) in this scenario represents a non-static solution. The Kerr-Newman black hole (KNBH) features a crucial ring singularity at $\Sigma = 0$, which corresponds to a special condition at $r = 0$. When the charge Q is set to zero, the line element and other quantities reduce to that of the Kerr black hole. In contrast, for zero rotation, the line element of the Reissner-Nordström black hole (RNBH) is fully recovered.

1.6 Hawking Radiation

Traditionally, black holes are thought to have so strong gravitational attraction that nothing, even electromagnetic radiation, can escape them. It is impossible for anything to return once inside. Thus, a black hole can expand over time.

1.6.1 Quantum Mechanics and Hawking Radiation

In 1974, Stephen Hawking made a revolutionary discovery about black holes. Building on the work of Jacob Bekenstein, who proposed that black holes have entropy and temperature, Hawking demonstrated that black holes can emit particles using quantum mechanical concepts. This emission, known as Hawking radiation, takes place close to the event horizon and is driven by quantum fluctuations along the black hole event horizon [12, 13].

1.6.2 Black Hole Evaporation

Hawking radiation has significantly altered our knowledge of black holes. Instead of being consuming creatures, black holes are now known to release radiation and lose mass over time. As a black hole emits Hawking radiation, it loses energy, causing its mass to steadily decrease. If a black hole loses enough mass through this mechanism, it will eventually evaporate, leaving no remains. A significant distinction exists between the thermal energy radiated from a black body and the radiation predicted by Hawking for black holes. Thermal radiation retains information about the emitting body, whereas Hawking radiation appears to lack such information. By the 'no-hair theorem', this discrepancy suggests that the characteristics of Hawking radiation are solely influenced by the BHs mass, angular momentum, and charge. This dilemma is known as the BH information paradox [12, 14].

1.7 Black Hole Thermodynamics

Thermodynamics is a branch of physics that deals with heat, energy, and how they move through or change in systems. Thermodynamics of BH is the study of BHs through the application of heat and energy laws. In addition to advancing our understanding of BHs, this research has given rise to new ideas regarding the possible connections between quantum mechanics and gravity, such as the idea that data about a black hole may be stored outside of it on its surface. It also tries to make a connection between the characteristics of BHs, particularly their event horizons, and the laws of thermodynamics, which explain heat and energy.

For the validity of the second law of thermodynamics, BHs need to have entropy. The basic principle that entropy constantly grows would be broken if BHs had no entropy, leading to a scenario in which the universe's overall entropy decreased. Because entropy grows with the size of the BHs event horizon, the universe's total entropy also grows, by the second law of thermodynamics.

According to Jacob Bekenstein, entropy (a measure of disorder or hidden information) is present in BHs and is correlated with the size of the event horizon, which is the black hole's border. Additionally, he suggested that independent of what falls into them, black holes just have three properties: mass, charge, and spin. These concepts allowed us to better comprehend black holes and relate them to the rules of thermodynamics. Jacob Bekenstein postulated in 1973 that a BHs entropy is correlated with the size of its event horizon. He proposed that the constant of proportionality should be about equal to $\ln 2/0.8\pi$, or 0.276. If this value was not the real constant, according to Bekenstein, it should be quite near to it.[15]

Stephen Hawking discovered that black holes release thermal radiation the next year, in 1974. This radiation is now referred to as Hawking radiation, and it is associated with a certain temperature, known as the Hawking temperature. Bekenstein's idea was confirmed by Hawking using the principles of thermodynamics, which demonstrate a connection between energy, temperature, and entropy. He discovered that $1/4$ is the true constant of proportionality for black hole entropy.

Bekenstein implies that a black hole's entropy, which measures its disorder or information content, is proportional to its surface area rather than its volume. But the Bekenstein-Hawking formula is a development and improvement of Bekenstein's concept, which was created in collaboration with Stephen Hawking. It gives the relationship between entropy and surface area

and a precise formula for determining a black hole's entropy. The formula is

$$S = \frac{KA}{4\mathscr{L}_p^2}. \tag{1.15}$$

The entropy is represented by S, the event horizon area by A, the Boltzmann constant by K, and the Planck length (a concise length scale) by $\mathscr{L}_p^2$. Black holes follow four rules that define their behaviour. These regulations are similar to the laws of thermodynamics, which describe the behaviour of heat and energy. Stephen Hawking added to the laws after they were initially found by James Bardeen, Brandon Carter, and Jacob Bekenstein. A unified spacetime measuring system illustrates the Laws of BH mechanics, making calculations simpler [16, 17, 18].

1.7.1 The Zeroth Law

When considering a stationary BH, the horizon's surface gravity remains constant. The zeroth law of thermodynamics and the zeroth law of BH mechanics are comparable. According to thermodynamics, an object's temperature is constant everywhere if it is in thermal equilibrium. According to this law, the surface gravity of a stable BH is the same anywhere on its event horizon. Surface gravity is similar to the gravitational attraction of a BH. Over a stationary BH's horizon, the surface gravity stays constant, just as temperature is in a stable system.

1.7.2 The First Law

The following relationship applies to stationary black holes: changes in area, angular momentum, and electric charge are correlated with energy changes.

$$dE = \frac{k_s}{8\pi} dA + \Omega dJ + \Phi dQ, \tag{1.16}$$

where dE represents the change in the BHs energy. Under general relativity, a BHs energy is proportionally linked to its mass; hence, this energy change is related to the BHs mass k_s denotes the surface gravity of the BH, dA indicates the change in the area of the BHs event horizon. Ω refers to the angular velocity at the BHs horizon, dJ shows the change in the BHs angular momentum, Φ represents the electric potential at the BHs horizon, dQ denotes the change in the BHs electric charge.

A system's overall energy is affected when heat is added, which changes the system's temperature, or when the system's disorder, or entropy, increases. The relationship between the

change in entropy and temperature and the change in energy is demonstrated by the equation $dE = TdS$.

1.7.3 The Principle of the Second Law

The complete entropy of a closed system always rises or remains constant over time in any natural process. It never decreases. It was believed that the black hole's horizon should never shrink in size. Considering that the horizon area equals entropy, then this area should always increase or remain the same, which is why this concept is comparable to thermodynamics' second law. This can be stated as

$$\frac{dA}{dt} \geq 0. \tag{1.17}$$

Hawking's research demonstrated that black holes can release radiation, or "Hawking radiation," which causes the holes to lose mass and energy. The BHs mass and horizon area both diminish as a result of this emission.

The second law of thermodynamics seemed to be broken if the horizon area of a BH could contract. The generalized second law of thermodynamics (GSL) was developed to address this. The BHs entropy and the entropy of the surrounding universe are combined in the *GSL*. It says that the total entropy of the universe, which includes the BH, never diminishes when considering both the entropy inside and outside of it. This implies that even in the presence of Hawking radiation, the second rule of thermodynamics remains valid.

1.7.4 The Third Law of Thermodynamics

When the temperature becomes closer to absolute zero, the entropy of a flawless crystal should approach 0, according to the third law of thermodynamics. Since real materials aren't perfect crystals and achieving absolute zero isn't feasible, applying this law is complicated at low temperatures due to quantum phenomena. For applied thermodynamics, this makes the third law less helpful. There is controversy around the third law of black hole thermodynamics because many unique black holes contradict the established theories [13, 18].

1.8 Dark Energy and Dark Matter

1.8.1 Dark Energy

The accelerated expansion of the universe is widely attributed to dark energy, a mysterious form of energy that permeates all of space and exerts a repulsive force on cosmic structures. Unlike ordinary matter and energy, which attract each other through gravitational interaction, dark energy is believed to possess negative pressure, resulting in a repulsive gravitational effect that drives galaxies apart.

Edwin Hubble observed very distant galaxies, or collections of stars far from us, in the 1920s with a large telescope [19]. His observations revealed what is known as "redshift"(a stretch toward the red end of the spectrum), which is the term used to describe how much light is emitted from these far-off galaxies. Redshift is the phenomenon of something moving away from us. Hubble discovered that these galaxies were veering away from our galaxy. He concluded that the universe was expanding since this indicated that the distance between galaxies was growing. Initially, scientists believed that the cosmos was growing steadily or that it was expanding at a constant rate. They also thought that the expansion might eventually slow down because of gravity, the force that holds stuff together [20, 21, 22].

This is because gravity would resist the expansion and force every constricts again. Two separate groups of astronomers made a significant discovery in 1998. They saw that the universe was expanding more slowly in the distant past than it is now.

Galaxies are accelerating in their motion away from us gradually. This indicates that the cosmos is expanding faster than it was before, and it is not just expanding at a constant rate. Scientists concluded that this rapid expansion had to be caused by something. Dark energy is the term they gave to this enigmatic reason. Because dark energy contains negative pressure, which pushes things apart rather than together, it differs from conventional matter.

Albert Einstein proposed the concept of the cosmic constant as a parameter in his general relativity equations. It was first included to accommodate the idea of a static universe in which nothing changes over time. Scientists looked again at the cosmological constant after finding evidence of accelerated expansion in 1998. It was suggested that the gravitational forces that push objects apart could be caused by this constant. According to the theory, dark energy, which exists in space itself, uniformly fills the universe. There were differences in the expected amount

of dark energy because the cosmological constant model's predictions and observations did not line up exactly [23, 21].

Einstein's equations contain a mathematical term called the energy-momentum tensor. Adding negative pressure to this term is one way to model dark energy. Different dark energy models suggested by this approach include quintessence, k-essence, perfect fluid models, and other theories based on particle physics. The dark energy model known as Quintessence postulates that the energy density of dark energy varies over space and time. A "scalar field," or a field that can have varying values at various points in space and time, is the kind of field used in this concept. This field and its associated energy cause the cosmos to expand faster. A different theoretical explanation for dark energy that bases its explanation of the universe's acceleration on the kinetic energy of a scalar field is called K-Essence [24, 25].

The kinetic and potential energies of the scalar field in k-essence can have a complicated relationship that impacts the universe's expansion. Dark energy is explained by perfect fluid models, which use the idea of a "perfect fluid," or a hypothetical fluid with an idealized pressure-density ratio. A different strategy is to alter the theories of gravity themselves. This method introduces functions of the Ricci scalar R, changing the behavior of gravity on cosmic scales and modifying Einstein's general relativity. Adding additional scalar fields that potentially influence the universe's expansion, scalar-tensor theories expand on general relativity [26, 27].

1.8.2 Dark matter

Swiss astronomer Fritz Zwicky noticed in the 1930s that galaxies in clusters were traveling far more quickly than was predicted. Concluding these speeds, he proposed that the clusters must be held together by an additional gravitational attraction from an unknown mass, or what he called "dark matter" [28].

American astronomer Vera Rubin examined the speed at which galaxies rotated throughout the 1970s. With the quantity of visible matter in those galaxies, she discovered that the stars near their edges were moving more quickly than they should have. This difference supported the theory of dark matter by indicating the existence of extra mass that is not visible [29].

Additional support for dark matter came from studies of the Cosmic Microwave Background (CMB), which is the remnant of the Big Bang. Temperature variations were observed in the CMB data, which were only clarified in the presence of dark matter.

Observations of the large-scale structure of the universe and galaxy formation in the 2000s demonstrated the critical role dark matter plays in forming the universe. It influences the formation and evolution of galaxies and helps them maintain their structure.

Through experiments on Earth and in space, scientists are still attempting to directly discover dark matter. Although no direct discovery of dark matter particles has been verified to date, they are searching for indications of their interactions with ordinary matter.

The Weakly Interacting Massive Particles (WIMPs) theory, which postulates the existence of theoretical particles with extremely weak interactions with conventional matter, is one prevailing theory explaining dark matter. Axions and sterile neutrinos, among other hypotheses and particles, could also be used to explain dark matter [30, 31].

CHAPTER 2

LITERATURE REVIEW

2.1 Introduction

Black holes have been an important topic in general relativity, with many changes and improvements made over time. The Kerr-Newman-Kiselev metric, which includes the effects of quintessence, has gained much attention because of its role in astrophysics and theoretical studies. This chapter discusses the history of black hole research, from early ideas to recent developments in the field.

In a letter written in November 1784 and later published, English astronomer and theologian John Michell speculated about the existence of an enormous celestial body so dense that even light couldn't escape from it. Michell made a valid observation when he said that these supermassive yet non-radiating bodies may be found by their gravitational pull on nearer visible bodies. He explained this idea using the fundamentals of Newtonian mechanics. Because light has a limited speed, Michell concluded that if a star's escape velocity (the speed required to escape the star's gravitational pull) were higher than the speed of light, the star's light would not reach an observer and would be invisible [32].

Several scientists were thrilled when John Michell first proposed the possibility of massive, undetectable "dark stars". But in the early 1800s, researchers realized light behaves more like a wave than a particle. This new understanding confused them about how gravity would affect light waves. They were unable to explain how gravity would capture light if it behaved like a

wave, thus their enthusiasm for the concept of "dark stars" vanished. According to Michell's theory, a light beam may emerge from a supermassive star, slow down due to the star's gravity, come to a stop, and then return to the star. However, the modern theory of gravity called general relativity, proves that this idea is incorrect. Rather, the curvature of spacetime ensures that light always travels on the same geodesic, which never leaves the "star" (black hole) surface [33, 34].

A similar conclusion was independently reached at the same time by Pierre-Simon Laplace, A renowned French astronomer and mathematician. In "Exposition du Système du Monde," published in 1796, Laplace suggested that there might be things in the cosmos with so much gravity that light cannot escape [35]. The 19th century experienced significant developments in the fields of physics and astronomy. Light's wave nature got more acceptance, particularly as a result of studies conducted by Augustin-Jean Fresnel and Thomas Young. Michell's particle-based theory of gravity became less significant in the scientific discussion of the day as a result of this change. Black holes and other such things were not directly observed. In those days, physics and astronomy were mostly concerned with analyzing evident phenomena, such as, and the nature of light [33].

Significant advancements in various scientific fields, including thermodynamics, atomic theory, and electromagnetic, occurred in the 19th century. The fast-developing branches of science took the attention of scientists, giving less room for hypothetical theories on subjects such as "dark stars". Before Einstein's general theory of relativity, scientists were unable to fully understand how large objects affected light and bent spacetime. With a more solid scientific foundation, this new knowledge sparked interest in Michell's original theory once again. While "BH" was not used, Michell and Laplace's "dark stars" established the foundation for the contemporary understanding of BHs. Only in the 20th century, When Albert Einstein introduced his theory of general relativity and established the essential framework to comprehend these mysterious things completely, was their work ignored. The warping of spacetime by heavy objects was explained by Einstein's equations [36].

During the year 1915, Einstein presented his revolutionary model of gravity, which provided a new model for explaining gravity. Einstein's work redefined gravity as the warping of spacetime influenced by mass and energy, in contrast to the previous Newtonian perspective, which considered gravity as a force between masses. This theory holds that spacetime is bent around enormous objects like stars and planets and that this curvature influences the paths that other things (including light) take [37]. Gravity could affect the speed of light, as Einstein had already

shown. He postulated in 1911 that light would be bent by a huge object's gravitational field when it passed close by. In 1919, a solar eclipse provided experimental confirmation of Einstein's theory when it was noticed that starlight bending near the Sun corresponded with the theory.

This idea was important because it established the theoretical foundation for understanding black holes by explaining how huge objects may capture light. According to Einstein's general theory of relativity, an object's gravitational attraction could become so powerful that not even light could escape if it were compact enough [38]. The development of general relativity changed Michell's idea of "dark stars" into a serious scientific theory. It showed that these objects are not just theoretical but possible and likely results of stellar evolution under certain conditions. Einstein's work provided the math needed to explore these ideas further. This established the groundwork for current research on black holes [32]. A few months later, Karl Schwarzschild solved the Einstein field equations, which describe the gravitational field around both a point mass and a spherical mass. Around the same time, Johannes Droste, a student of Hendrik Lorentz, independently arrived at the same solution for a point mass and provided a more detailed analysis of its properties. Shortly after the discovery of general relativity by Albert Einstein, Karl Schwarzschild made a major contribution to the field. A group of ten connected differential equations make up Einstein's field equations. Finding precise solutions to them is very difficult because they are complex and highly nonlinear [39]. Schwarzschild solved these equations by making several simplifying assumptions.It is assumed that the mass that generates the gravitational field is non-rotating and completely spherical. He found a solution outside the mass in space, where no matter exists. He solved the equations and derived a solution. This result is referred to as the Schwarzschild metric. The Schwarzschild metric describes how spacetime is curved by a spherical mass. At a certain distance (now known as the Schwarzschild radius) from the center of a mass, Schwarzschild's solution exhibited peculiar behavior. Einstein's equations stop functioning normally at this radius because some of the terms become infinite. Scientists were still figuring out what this surface represented at the [40]. Different coordinates could solve the infinite terms in the Schwarzschild solution, as Arthur Eddington found in 1924 the equations appeared to break down and produce infinite solutions near the Schwarzschild radius, which was confusing. Eddington demonstrated that the issue vanished when positions in space were measured using new coordinates. This indicated that the singularity at the Schwarzschild radius was brought on by the initial coordinate selection rather than an actual physical problem. This knowledge helps in the scientific study of BHs [41]. It

was discovered by Georges Lemaitre in 1933 that the singularity at the Schwarzschild radius was a function of the coordinates chosen rather than a genuine physical issue. When a star's mass is squeezed down to its Schwarzschild radius was theorized by Arthur Eddington in his book from 1926. Based on Einstein's hypothesis, he mentioned that a star of that kind could not have the same high density as the Sun. If this occurred, space would bend around the star so much that it would become invisible to us, the gravity would be so great that light could not escape, and the spectrum of light would shift completely [11]. Subrahmanyan Chandrasekhar made a significant discovery in 1931 that changed our understanding of black holes. He discovered that a non-rotating star formed by dense objects, such as white dwarf stars, cannot remain stable above a specific mass. This value, approximately 1.4 times the Sun's mass, is referred to as the Chandrasekhar limit [42]. The discovery made by Chandrasekhar was significant since it demonstrated that not all stars have the ability to decay into white dwarfs. A star must collapse further if its mass exceeds the Chandrasekhar limit after exhausting its fuel. This theory clarified the formation process of neutron stars and BHs for scientists [43].

Many scientists, especially Lev Landau and Arthur Eddington, criticized Chandrasekhar's theory. They considered that an unidentified force would prevent a star from fully collapsing. Their assumption was partly accurate; when a white dwarf's mass slightly surpasses the Chandrasekhar limit, it undergoes collapse but stabilizes as a neutron star rather than continuing to contract [44]. A neutron star is an extremely dense object that forms when a big star burns out of nuclear fuel. It is extremely compact, but unless it is even more massive, it does not collapse into a black hole. The Tolman–Oppenheimer–Volkoff (TOV) limit is the point at which a neutron star will continue to collapse into a BH if its mass exceeds it, according to a 1939 prediction by Robert Oppenheimer and his associates. This theory expanded upon previous research by Chandrasekhar, which demonstrated that certain stars lose their stability at a given mass [45]. Based on the Pauli Exclusion Principle, which describes why particles such as electrons cannot belong to the same space, their first calculations indicated that this limit was approximately 0.7 solar masses. The strong force, which holds neutrons together, was later taken into consideration, and it was discovered that this limit might be higher between 1.5 and 3 times the solar mass. Based on the analysis of GW170817 data, scientists have improved our understanding of the TOV limit, estimating it to be approximately 2.17 times the solar mass. This means that if the mass of a neutron star is greater than this limit, the intense gravitational pull of the sun will almost certainly cause it to collapse into a black hole because the internal forces of the star will

no longer be able to balance the force [46]. Oppenheimer was researching the consequences of a large star collapsing due to its gravity. They discovered that the collapse would continue if the star's mass was high enough until the star's size shrank to its Schwarzschild radius. At this radius, the star turns into a BH, and the event horizon denotes the point beyond which nothing can escape. Their calculations show that time acts quite strangely when the star gets closer to this event horizon. When the star approaches this point, time appears to slow down more and more to an observer far from it. From the perspective of the distant viewer, time seems to freeze altogether when the star reaches the Schwarzschild radius. This would give the impression that the star was "frozen" in time, on the edge of turning into a black hole.

When a person is falling into a star, time appears to pass normally, and they are unaware of any unexpected occurrences as they cross the event horizon. An important idea in general relativity is the variation in how time is experienced based on one's position.

The concept behind the name "frozen star" is that the star appears to be frozen at the precise instant it turns into a black hole, giving the impression that it is stuck in space. However, the intense gravitational pull on time close to the event horizon is only an illusion, giving the appearance of anything "frozen" [47].

In a paper titled "On a Stationary System with Spherical Symmetry Consisting of Many Gravitating Masses," published in 1939, Albert Einstein attempted to use his theory of general relativity to deny the existence of BHs. Black holes, in his opinion, are not real [48]. Only a few months later, on the other hand, a different scientist named Robert Oppenheimer and his student Hartland Snyder released a paper titled "On Continued Gravitational Contraction." Black hole formation was demonstrated through the use of Einstein's theory. The idea of black holes was seriously predicted for one of the first occasions in the history of modern science. They showed that black holes may exist, so rejecting Einstein's recent study, which they neglected to mention in their work [49, 48].

David Finkelstein discovered something significant about black holes in 1958. He recognized the Schwarzschild surface as an event horizon, which is the edge surrounding a black hole. A one-way membrane, such as an event horizon, through which light can only enter and never leave. Rather than contradicting what Oppenheimer had previously stated, this theory gave further insight, particularly when considering one's perspective of a person falling into a BH [50, 51].

In 1967 pulsar discovery by Jocelyn Bell Burnell significantly impacted this shift [52, 53]. Scientists discovered in 1969 that pulsars were neutron stars spinning quickly. Black holes and

neutron stars were previously only considered hypothetical ideas. However, the discovery of pulsars demonstrated the reality of these things and increased curiosity about the variety of dense objects that could arise from gravitational collapse [54].

The understanding of black holes was greatly advanced by physicists in the early 1960s. The exact mathematical solution, or Kerr solution, was discovered in 1963 by Roy Kerr and describes a rotating black hole. This work was expanded upon two years later, in 1965, when Ezra Newman solved the problem of a revolving black hole with an electrical charge. The Kerr-Newman solution is the name given to this approach [55].

The work of Werner Israel [56], Brandon Carter [57] and David Robinson [58] helped to shape the "no-hair theorem," which was developed with the help of these discoveries. According to the theorem, three characteristics are sufficient to characterize a stationary BH: Its gravitational mass, electrical charge, and rotational energy, which is connected to its spin. In other words, black holes have no additional "features" or "hair" than these three, which is why the term "no-hair theorem" developed. Due to this concept, black holes were easier to explain and scientists were able to concentrate their research on these crucial variables [59].

The belief that singularities, or places where gravity becomes infinitely strong, which are observed in black hole solutions, are merely mathematical variations resulting from particular conditions used during calculations, and that they would not occur in most real-world scenarios, has been confirmed by the work of scientists such as Vladimir Belinsky, Isaak Khalatnikov, and Evgeny Lifshitz [60].

When a star falls under the force of gravity, singularities can occur in a variety of circumstances, as demonstrated by Roger Penrose and Stephen Hawking in the 1960s [61]. Their ground-breaking research contributed to the acceptance of the reality of black holes, with their singularities, as more than only strange theoretical concepts. For this study, Penrose received half of the 2020 Nobel Prize in Physics (Hawking died in 2018) [62].

During the early 1970*s*, investigations of Cygnus X-1, a cosmic X-ray source identified in 1964, led scientists to generally recognize it as the first known BH. This demonstrated that BHs do exist in the universe [63].

The theory of BH thermodynamics was developed in the early 1970*s* by scientists James Bardeen, Jacob Bekenstein, Brandon Carter, and Stephen Hawking. This theory explains how black holes act in ways that are comparable to how heat, energy, and work are governed by the principles of thermodynamics. For instance, they discovered that the mass of a BH is correlated with energy,

the surface area with entropy, a measure of disorder, and the temperature with surface gravity [13].

In 1974, Hawking demonstrated that black holes should, by quantum field theory, produce radiation, just like a stove radiates heat. This strengthened the connection even more. Hawking radiation is the name given to this type of radiation that indicates black holes can gradually lose mass and energy [12].

On February $11, 2016$, researchers from the Virgo and LIGO collaborative research confirmed the first direct measurement of gravitational waves. The merger of two black holes produced these waves, which were the first of their kind to be seen [64].

Then, using data from the Event Horizon Telescope (EHT), astronomers published the first direct photograph of a black hole on April $10, 2019$. This photograph displayed the Messier 87 galaxy's supermassive black hole in its center [65].

Approximately $1,560$ light-years away, Gaia BH1 is the closest BH currently believed to exist in 2023. In the Milky Way, scientists believe there are hundreds of millions more black holes than the few dozen that have been discovered. Because they don't release radiation and can only be found by their gravitational pull on nearby objects, the majority of these black holes are probably single [66].

CHAPTER 3

TOPOLOGICAL CLASSE BLACK HOLE IN PFDM BACKGROUND

3.1 Introduction

The black hole is a topic of interest for many researchers from both theoretical and observational physics. Recently, there was a significant breakthrough in astronomy in the study of BH shadows [67]. The thermodynamics of BHs has been a subject of research for many years, with various aspects extensively studied in the literature. For a better understanding of the thermodynamic behavior of black holes, a recent proposal has been made based on the concept of off-shell energy and its treatment as topological thermodynamic defects. They suggested that from the off-shell free energy $\mathscr{F}$ (which is the difference between the BH mass and the product of the entropy and temperature) we can define a vector field whose radial component is the derivative of off-shell free energy for event horizon radius parameter r_h. In another, paper a residual-based approach has been given [5]. Therefore, the topological number is a useful tool for a better understanding of black hole physics.

Recently, in 2022 the Wei *et al.* [5] classified the BH into three topological classes based on the topological classes. They proposed that all the BHs can be classified into one of 3 classes for which the sum of the winding number is $-1, 0, 1$. The mentioned study is based on the concept of winding numbers which an integers representing the total number of times that the curve travels counterclockwise around the zero point, that is, the curve's number of turns corresponds

to the sum of the winding numbers of the vector field's zero points, resulting in the topological number.

Now, we talk about the "off-shell free energy of the thermodynamical system," it typically refers to the thermodynamic properties and free energy of the system when they are not in their equilibrium states. In other words, it's related to considering systems when the change in the properties of the system is allowed. This concept is used in various theoretical physics contexts. For example, a BH can be considered a thermodynamical system with well-define attributes like Hawking temperature and entropy (Entropy is a measure of a system's disorder or randomness), and the study of BH thermodynamics, particularly in the context of Hawking radiation, where the creation and evaporation of virtual particles near the event horizon are considered is very important.

In the next section, we examine the process of identifying the topological number of Kerr BHs. For this purpose, we consider Kerr BH whose line element can be expressed as [68],

$$\begin{aligned} ds^2 = &-\frac{\Delta}{\Sigma}\left(dt - a\sin^2\theta d\phi\right)^2 + \frac{\Sigma}{\Delta}dr^2 + \Sigma d\theta^2 \\ &+\frac{\sin^2\theta}{\Sigma}\left[adt - (r^2+a^2)d\phi\right]^2, \end{aligned} \tag{3.1}$$

where

$$\Delta = r^2 - 2mr + a^2, \quad \Sigma = r^2 + a^2\cos^2\theta. \tag{3.2}$$

Here, m indicates mass, and a refers to the spinning parameter of Kerr BHs. To evaluate the thermodynamic spacetime defined by (3) are as follows,

$$\begin{aligned} M = m, \quad \Omega = \frac{a}{r_h^2 + a^2}, \\ S = \pi\left(r_h^2 + a^2\right), \quad T = \frac{r_h^2 - a^2}{4\pi r_h\left(r_h^2 + a^2\right)}, \end{aligned} \tag{3.3}$$

The parameter m defines the black hole's geometric mass in the metric, while M represents its physical mass measured by a distant observer. The position of the horizons of BHs defined by (3) is given as $r_h = m \pm \sqrt{m^2 - a^2}$. At this point, our focus shifts to investigating the topological value of Kerr BHs by using the expression of thermodynamic quantities mentioned above. According to Ref [5], First, we introduce the modified off-shell energy of a BH

$$\mathscr{F} = M - \frac{S}{\tau}, \tag{3.4}$$

Here M is mass S is entropy, and τ refers to the inverse temperature associated with the cavity near the Kerr BHs. It is assumed that a vector ϕ is

$$\phi = \left(\frac{\partial \mathscr{F}}{\partial r_h} \ , -\csc\theta \ \cot\theta \right), \tag{3.5}$$

where the angular parameter is in the range $0 \leq \theta \leq \pi$. It is possible to derive the origin of the vector field by setting $\phi = 0$ or in other words ϕ^{r_h} and ϕ^{θ}.

Now we define off-shell free energy in terms of BH horizon parameter r_h. For that purpose, we express the mass M and entropy S in terms of the BH horizon parameter r_h. This can be done by setting the horizon equation equal to zero, that is, $\Delta(r_h) = 0$. which yields the following equation,

$$r_h^2 - 2mr_h + a^2 = 0. \tag{3.6}$$

For the above equation for m, we get

$$m = \frac{r_h^2 + a^2}{2r_h}, \tag{3.7}$$

For the thermodynamical quantities, we can see that for the Kerr BH, $m = M$, and therefore, in the case the off-shell free energy as a function of the BH horizon parameter can be formulated as,

$$\mathscr{F} = \frac{r_h^2 + a^2}{2r_h} - \frac{\pi\left(r_h^2 + a^2\right)}{\tau}, \tag{3.8}$$

We know that,

$$\phi^{r_h} = \frac{\partial \mathscr{F}}{\partial r_h}, \tag{3.9}$$

$$\frac{\partial \mathscr{F}}{\partial r_h} = \frac{\partial}{\partial r_h}\left(\frac{r_h^2 + a^2}{2r_h}\right) - \frac{\partial}{\partial r_h}\left(\frac{\pi\left(r_h^2 + a^2\right)}{\tau}\right),$$

So, in this case, the components of vectors ϕ become

$$\phi^{rh} = \frac{1}{2} - \left(\frac{a^2}{2r_h^2}\right) - \frac{2\pi r_h}{\tau}, \tag{3.10}$$

$$\phi^{\theta} = -cot\theta \csc\theta, \tag{3.11}$$

Now, to find the inverse temperature parameter, we set $\phi^{r_h} = 0$, to get the expression for component τ that is an extra variable for Kerr BH.

$$\tau = \frac{4\pi r_h^3}{r_h^2 - a^2}. \tag{3.12}$$

Keep in mind that τ should exceed τ_c, for example, $\tau = 34.48$ and $a = 1$ in *Figure* 3.9, At which two zero points occur: $ZP1$ at $r_h = 1.46r_0$ and $ZP2$ at $r_h = 2.15r_0$, having the winding numbers $\omega_1 = 1$ and $\omega_2 = -1$, correspondingly. As a result, one can calculate the topological number $W = 0$ for the four-dimensional Kerr BH.

This inverse temperature parameter plays an important role in the topological number. It can be shown that the Kerr and RN BHs have the same topological number as zero [5]. On the other hand, the topological number of the Schwarschild BH is -1. It means that the rotation parameter has played a key role in thermodynamic behavior and classification based on topological numbers.

In our research, we explore how the magnetic field and other parameters affect these numbers and what are the significance of these numbers in the BH thermodynamics.

3.1.1 Higher Dimensional Rotating BHs

Since most astrophysical black holes are rotating, and the dimensionality of spacetime affects their properties, studying the topological behavior of higher-dimensional rotating black holes is important for understanding their nature and testing recent theoretical predictions. Now, we move on to exploring rotating BHs in higher dimensions, with a particular emphasis on d-dimensional singly rotating Kerr BHs. The metric for these black holes in arbitrary dimensions is as follows [69, 70]

$$\begin{aligned} ds^2 = &-\frac{\Delta r}{\Sigma}\left(dt - a\sin^2\theta d\phi\right)^2 + \frac{\Sigma}{\Delta r}dr^2 + \Sigma d\theta^2 \\ &+\frac{\sin^2\theta}{\Sigma}\left[adt - (r^2+a^2)d\phi\right]^2 + r^2 cos^2\Omega^2_{d-4}, \end{aligned} \tag{3.13}$$

where $d\Omega_d$ represents a d-dimensional unit sphere's line element and

$$\Delta r = r^2 - 2mr^{5-d} + a^2, \quad \Sigma = r^2 + a^2 cos^2\theta, \tag{3.14}$$

If we substitute $\Delta r = 0$ into Equation (1.14), we can determine the value of m. This value can then be used in the expression for M to complete the calculation.

where,

$$M = \frac{d-2}{8\pi} w_{d-2} m, \tag{3.15}$$

putting the value of m we get,

$$M = \frac{d-2}{8\pi} w_{d-2} \left(\frac{r_h^2 + a^2}{2r_h^{5-d}}\right), \tag{3.16}$$

The thermodynamic quantities are [70]

$$J=\frac{\omega_{d-2}}{4\pi}ma \quad \Omega=\frac{a}{r_h^2+a}, \quad S=\frac{\omega_{d-2}}{4}(r_h^2+a^2)r_h^{d-4}, \tag{3.17}$$
$$T=\frac{r_h}{2\pi}\left(\frac{1}{r_h^2}+\frac{d-3}{2r_h^2}\right)-\frac{1}{2\pi r_h},$$

By using Equation (1.17), we can determine the value of the generalized free energy,

$$\mathscr{F}=\frac{d-2}{8\pi}\omega_{d-2}\left(\frac{r_+^2+a^2}{2r_+^{5-d}}\right)-\frac{\omega_{d-2}}{4\tau}(r_+^2+a^2)r_+^{d-4}, \tag{3.18}$$

The vector component ϕ can be computed as we know that $\phi=\frac{\partial\mathscr{F}}{\partial r_h}$ So take the partial derivative of $\mathscr{F}$ with respect to r_h we will get,

$$\phi^{rh}=\frac{\omega_{d-2}r^{d-6}}{16\pi\tau}\Big\{(d-2)\big[(d-3)\tau-4\pi r_h r_h^2\big] \\ +a^2\big[\tau(d-2)(d-5)-4(d-4)\pi r_h\big]\Big\}. \tag{3.19}$$

$$\phi^{\theta}=-\cot\theta\csc\theta, \tag{3.20}$$

One can achieve $\phi^{rh}=0$ by solving the equation.

$$\tau=\frac{4\pi[(d-2)r_h^3+(d-4)a^2r_h]}{(d-2)[(d-3)r_h^2+(d-5)a^2]}, \tag{3.21}$$

Using *Figure* 3.10, the topological numbers associated with higher-dimensional Kerr BHs with single rotation are derived. For example, the topological number associated with a five-dimensional Kerr BH is determined using the corresponding metric and topological analysis $W=-1+1=0$, aligning with the result for the four-dimensional Kerr BH. We observe that the topological number differs for $d\geq 6$ compared to $d=4$ and $d=5$, representing two distinct topological classes of singly rotating Kerr BHs. So we conclude that the dimension of space-time plays key a role in the topological number of the rotating BHs, so it is reported in Ref [5]. in Lovelock gravity theory of higher–dimensional static uncharged BH.

3.1.2 Kerr-Newman Black Hole

We now investigate how the electric charge parameter influences the topological number of four-dimensional rotating BHs in the context of pure Einstein-Maxwell gravity. In the following

section, we specifically examine the topological number associated with a five-dimensional Kerr BH [71, 72], considering its metric and Abelian gauge potential.

$$ds^2 = \frac{\Delta_r}{\Sigma}(dt - asin^2\theta d\phi)^2 + \frac{\Sigma}{\Delta_r}dr^2 + \Sigma d\theta^2 + \frac{sin^2\theta}{\Sigma}[adt - (r^2+a^2)d\phi]^2. \tag{3.22}$$

$$A = \frac{qr}{\Sigma}(dt - asin^2\theta d\phi). \tag{3.23}$$

where,

$$\Delta = r^2 + a^2 mr + q^2, \quad \Sigma = r^2 + a^2 cos^2\theta, \tag{3.24}$$

In this context, m refers to the mass parameter, while a and q denote the parameters for spin and electric charge, respectively. The thermodynamic properties can be derived through the conventional calculation method, as explained below.

$$M = m, \quad J = ma, \quad \Omega = \frac{a}{r_h^2 + a^2}, \quad Q = q, \quad \phi = \frac{qr}{r_h^2 + a^2},$$
$$S = \pi(r_+^2 + a^2), \quad T = \frac{r_h^2 - a^2 - q^2}{4\pi r_h(r_h^2 + a^2)} \tag{3.25}$$

where $\Delta = 0$. So, for Kerr-Newman BH generalized free energy is

$$\mathscr{F} = M - \frac{S}{\tau} = \frac{r_h^2 + a^2 + Q^2}{2r_h} - \frac{\pi(r_h^2 + a^2)}{\tau}, \tag{3.26}$$

we know that,

$$\phi^{rh} = \frac{\partial \mathscr{F}}{\partial r_h} = \frac{\partial}{\partial r_h}\frac{r_h^2 + a^2 + Q^2}{2r_h} - \frac{\partial}{\partial r_h}\frac{\pi(r_h^2 + a^2)}{\tau}, \tag{3.27}$$

Then we will get

$$\phi^{rh} = 1 - \frac{r_h^2 + a^2 + Q^2}{2r_h^2} - \frac{2\pi r_h}{\tau}, \tag{3.28}$$

$$\phi^{\theta} = -cot\theta csc\theta, \tag{3.29}$$

$$\tau = \frac{4\pi r_h^3}{r_h^2 + a^2 - Q^2}, \tag{3.30}$$

It is an important parameter in studying the topological class of BH. *Figure* 3.7 Demonstrates the locations where the component ϕ^{rh} reaches zero for $a = r_0$ and $Q = r_0$, while *Figure*3.8

depicts the vector field n with unit magnitude under the conditions $\tau = 50r_0$, $a = r_0$, and $Q = r_0$. From these figures, For the four-dimensional Kerr-Newman BH, the topological number is found to be $W = 0$, which matches the result obtained for the four-dimensional Kerr BH in the second section and the five-dimensional singly rotating Kerr BH in the third Section. Furthermore, this suggests that the electric charge parameter does not play a role in determining the topological number of rotating BHs. Nevertheless, this hypothesis requires further validation through an analysis of the topological numbers of other rotating-charged BHs.

3.1.3 Kerr-Newman BHs under the Influence of PFDM

Let us start by reviewing that the action governing gravity theory with minimal PFDM coupling can be used to calculate the metric for a BH in PFDM

$$\mathscr{J} = \int dx^4 \sqrt{-g} \left(\frac{1}{16\pi G} R + \mathscr{L}_D M \right), \tag{3.31}$$

then using the field equations of Einstein, the result was obtained as

$$R_{\mu\nu} - \frac{1}{2} g_{\mu\nu} R = 8\pi G T^{DM}_{\mu\nu}, \tag{3.32}$$

PFDM's effective energy density, which is provided by

$$T^t_t = T^r_r = \frac{1}{8\pi} \frac{\alpha}{r^3}, \tag{3.33}$$

After obtaining the static solution, the Newman-Janis method can be utilized to derive the line element of a Kerr-Newman BH under the influence of dark matter, which is expressed as follows [73]

$$\begin{aligned} ds^2 = &- \left(1 - \frac{2mr - \alpha r \ln\left(\frac{r}{|\alpha|}\right)}{\Sigma} \right) dt^2 + \frac{\Sigma}{\Delta_r} dr^2 + \Sigma d\theta^2 - 2a \left(\frac{2mr - \alpha r \ln\left(\frac{r}{|\alpha|}\right)}{\Sigma} \right) dt d\phi \\ &+ \sin^2\theta \left(r^2 + a^2 + a^2 \sin^2\theta \frac{2mr - \alpha r \ln\left(\frac{r}{|\alpha|}\right)}{\Sigma} \right), \end{aligned} \tag{3.34}$$

where,

$$\Delta_r = r^2 - 2mr + a^2 + \alpha r \ln\left(\frac{r}{|\alpha|}\right), \tag{3.35}$$

$$\Sigma = r^2 + a^2 \cos^2\theta, \tag{3.36}$$

In this scenario, α characterizes the influence of dark matter, m denotes the mass parameter, and a signifies the rotation parameter. This line element corresponds to a BH with two distinct horizons, an inner horizon (r_-) and an outer (Cauchy) horizon (r_h), for any given value of α, provided that $a < k_c$. The line element with $a = k_c$ represents an extremal BH with a single horizon. The PFDM parameter α determines the BHs size. In the PFDM background, the Kerr black hole is defined by its mass M, entropy S, and Hawking temperature T, described as follows [74]

$$M = m, \tag{3.37}$$

$$S = \pi(r_h^2 + a^2), \tag{3.38}$$

$$T = \frac{r_h}{4\pi(r_h^2 + a^2)}\left(1 - \frac{a^2}{r_h^2} + \frac{\alpha}{r_h}\right), \tag{3.39}$$

The modified off-shell free energy associated with this system in the given context is given by

$$\mathscr{F} = M - \frac{S}{\tau},$$

$$\mathscr{F} = \frac{1}{2r_h}\left[r_h^2 + a^2 + \alpha r_h \ln\left(\frac{r}{|\alpha|}\right)\right], \tag{3.40}$$

The ϕ component associated with the vector field can be expressed as

$$\phi^{rh} = \frac{1}{2r_h^2}\left(r_h^2 + \alpha r_h - a^2\right) - \frac{2\pi r_h}{\tau}, \tag{3.41}$$

$$\phi^{\theta} = -\cot\theta \csc\theta, \tag{3.42}$$

The Kerr black hole's inverse temperature parameter in PDFD can be expressed as

$$\tau = \frac{4\pi r_h^3}{r_h^2 + \alpha r_h - a^2} \equiv \mathscr{G}(rh), \tag{3.43}$$

The point where the n vector field ϕ becomes zero, or τ the parameter associated with inverse temperature, is shown to decrease as α increases. Plotting the vector field ϕ allows us to confirm our results for the winding number w_i and topological number W, which we found using the method described in [75]. Thus, a characterized complex function is defined as follows

$$\mathscr{R}(z) = \frac{1}{\tau - \mathscr{G}(z)}, \tag{3.44}$$

We define the winding number w_ι as [75]

$$w_\iota = \frac{Res\mathscr{R}(z_\iota)}{|Res\mathscr{R}(z_\iota)|} \equiv Sgn[Res\mathscr{R}(z_\iota)], \tag{3.45}$$

The sign function is represented by $Sgn(x)$, the absolute value of z is defined by $|z|$, and the residue of $\mathscr{R}(z_\iota)$ associated with the distinct point z_i is represented by $Res\mathscr{R}(z_\iota)$.

$$\mathscr{R}_(z) = -\frac{z^2+\alpha z-a^2}{4\pi z^3-\tau\left(z^2+\alpha z-a^2\right)} \equiv -\frac{z^2+\alpha z-a^2}{\mathscr{A}(z)}, \tag{3.46}$$

For any given value of α with $a < k_c$ and $\tau < \tau_c$, examining the roots of $\mathscr{A}(z) = 0$ reveals that

$$\tau_c = 4\pi\frac{\left(-\alpha+\sqrt{3a^2+\alpha^2}\right)^3}{2a^2-\alpha\left(-\alpha+\sqrt{3a^2+\alpha^2}\right)}, \tag{3.47}$$

There are two complex roots and one negative root. So, the off-shell requirement isn't clear. On the other hand, we have three singular points such that for $\tau_c < \tau$

$$z_1, z_2, z_3 \in \mathbb{R}, \quad 0 < z_2 < z_1 \quad \text{whereas} \quad z_3 < 0. \tag{3.48}$$

Consequently, the topological number and related winding numbers are

$$w_\iota = -1, w_2 = 1 \quad \text{and} \quad W = 0, \tag{3.49}$$

This demonstrates that the Kerr BH in PFDM has the same topological number and winding numbers as the Kerr BH [76]. The plotting of the unitary vector field n associated with the Kerr BH under the influence of PFDM in *Figure*3.6 also illustrates this. The vector field ϕ has its zero points denoted by black dots.

3.1.4 Dark Matter Background and Schwarzschild BH

The Schwarzschild BH in the PFDM context can be viewed as a particular for the Kerr BH under the influence of PFDM, from which the static line element can be derived.

$$ds^2 = -f(r)dt^2 + \frac{1}{f(r)}dr^2 + r^2\left(d\theta^2 + sin^2\theta d\phi^2\right), \tag{3.50}$$

with

$$f(r) = 1 - \frac{2m}{r} + \frac{\alpha}{r}\ln\left(\frac{r}{|\alpha|}\right), \tag{3.51}$$

In this case, α is the PFDM parameter and m is the mass. Keep in mind that the metric given in equation (1.50) describes a black hole possessing a single event horizon, denoted by r_h, for each choice of the parameter α. Moreover, as the dark matter parameter α increases, the event horizon's size does as well [77]. The Schwarzschild BHs thermodynamic quantities in the PFDM background can be represented as follows [74].

$$M = m, \quad S = \pi r_h^2, \quad T = \frac{1}{4\pi r_h}\left(1 + \frac{\alpha}{r_h}\right), \tag{3.52}$$

When the Schwarzschild black hole's thermodynamic quantities and the line element are absent (i.e., when $\alpha = 0$), the line element becomes the same. PFDM's generalized off-shell free energy for the Schwarzschild BH is as follows:

$$\mathscr{F} = \frac{1}{2}\left[r_h + \alpha \ln\left(\frac{r}{|\alpha|}\right)\right] - \frac{\pi r_h^2}{\tau}, \tag{3.53}$$

Moreover, the constituents of the field associated with the vector ϕ are

$$\phi^{r_h} = \frac{1}{2}\left(1 + \frac{\alpha}{r_h}\right) - \frac{2\pi r_h}{\tau}, \tag{3.54}$$

$$\phi^{\theta} = -\cot\Theta \csc\Theta, \tag{3.55}$$

It provides the values of the cavity surrounding the BHs inverse temperature parameter τ as

$$\tau = \frac{4\pi r_h^2}{r_h + \alpha}, \tag{3.56}$$

As α increases, the dark matter parameter τ decreases, as demonstrated by this. Additionally, the outcome becomes the Schwarzschild BH in the absence of PFDM $(\alpha = 0)$ [5]. The complex function that has been characterized is now provided as

$$\mathscr{F} = -\frac{z + \alpha}{4\pi z^2 - \tau(z + \alpha)}, \tag{3.57}$$

There are two singular points, let's say z_1 and z_2, in the expression $\mathscr{R}(z)$ considering all values of α such that

$$z_1, z_2, \in \mathbb{R}, \quad \text{and} \quad z < 0 \quad \text{whereas} \quad 0 < z_1, \tag{3.58}$$

Since the off-shell requirement cannot be met for the negative real root z_2, we can only take into account the positive singular value z_1, which provides the appropriate winding number w_1 and the topological number as

$$w_1 = -1 \quad \textit{and} \quad W = -1, \tag{3.59}$$

This shows that in the PFDM framework, the topological classes and winding number of the Schwarzschild BH are in line with those of the BH [5]. On the other hand, they deviate from the matching values for the Kerr BH under the influence of the PFDM setting. Therefore, in the framework of PFDM, spacetime's topological properties are impacted by its rotation. The graphical depiction of the field represented by the vector n in Fig. 3.5 provides evidence supporting this assumption.

3.1.5 Dark Matter and Its Impact on Kerr-AdS Black Holes

This part of the paper addresses how PFDM affects Kerr-Ads spacetime topological classes. According to the dark matter backdrop, the Kerr-Ads BHs line element is [73]

$$ds^2 = -\frac{\Delta_r}{\Xi\Sigma}\left(dt - asin^2\theta d\phi\right)^2 + \frac{\Sigma}{\Delta}dr^2 + \frac{\Sigma}{\Delta_\theta}d\theta^2 + \frac{\Delta_\theta \sin^2\theta}{\Xi\Sigma}\left[adt - \left(r^2+a^2\right)d\phi\right], \quad (3.60)$$

where

$$\Delta_r = r^2 - 2mr + a^2 - \frac{\Lambda}{3}r^2\left(r^2+a^2\right) + \alpha r \ln\left(\frac{r}{|\alpha|}\right), \quad (3.61)$$

$$\Delta_\theta = 1 + \frac{\Delta}{3}a^2\cos^2\theta, \quad (3.62)$$

$$\Delta = r^2 + a^2 cos^2\theta \quad \Xi = 1 + \frac{\Lambda}{3}a^2, \quad (3.63)$$

In this case, α is associated with the PFDM parameter, whereas Λ represents the cosmological constant.

The line element (4.62) illustrates a Kerr-AdS BH in the absence of PFDM $(\alpha = 0)$. The horizon equation can be solved to determine the locations of the BH horizons.

$$\Delta_r = r^2 - 2mr + a^2 - \frac{\Lambda}{3}r^2\left(r^2+a^2\right) + \alpha r \ln\left(\frac{r}{|\alpha|}\right) = 0, \quad (3.64)$$

The mass and further thermodynamic variables are provided by [74]

$$M = \frac{m}{\Xi^2}, \quad (3.65)$$

$$s = \frac{\pi\left(r_h^2 + a^2\right)}{\Xi}, \quad (3.66)$$

$$T=\frac{r_h}{4\pi\Xi\left(r_h^2+a^2\right)}\left[1-\frac{a^2}{r_h^2}-\frac{\Lambda}{3}\left(3r_h^2+a^2\right)+\frac{\alpha}{r_h}\right], \tag{3.67}$$

The system's generalized off-shell free energy can be derived by using these thermodynamic characteristics as

$$\mathscr{F}=\frac{1}{2\pi r_h\left(3-8\pi a^2P\right)^2}\left[3\left(r_h^2+a^2\right)\mathscr{G}+9\alpha r_h\tau\ln\left(\frac{r}{|\alpha|}\right)\right], \tag{3.68}$$

where

$$\mathscr{F}=2\pi r_h\left(8\pi Pa^2+4\tau Pr_h-3\right)+3\tau, \tag{3.69}$$

giving the n vector field's components as

$$\phi^{r_h}=\frac{6\pi r_h^2 8\pi a^2 r_h P-3r_h+2\pi P\left(a^2+3r_h^2\right)}{2r_h^2\tau\left(3-8\pi a^2P\right)^2}+\frac{9\tau\left(r_h^2+\alpha r_h-a^2\right)}{2\tau r_h^2\left(3-8\pi a^2P\right)}, \tag{3.70}$$

$$\phi^{\theta}=-\cot\Theta\csc\Theta, \tag{3.71}$$

Consequently, the Kerr-Ads BHs inverse temperature in PFDM is

$$\tau=\frac{4\pi r_h^3\left(3-8\pi a^2P\right)}{3\left(r_h^2+\alpha r_h-a^2\right)+8\pi Pa^2r_h^2\left(a^2+3r_h^2\right)}, \tag{3.72}$$

In this instance, the characterized function is

$$\mathscr{R}(z)\equiv-\frac{3\left(z^2+\alpha z-a^2\right)+8\pi Pa^2z\left(a^23z^2\right)}{\mathscr{A}(z)}, \tag{3.73}$$

where

$$\mathscr{A}(z)=4\pi z^2\left(3-8\pi Pa^2\right)-\tau\left\{3\left(z^2+az-a^2\right)+8\pi Pa^2z\left(a^2+3z^2\right)\right\}, \tag{3.74}$$

The examination of the roots of $\mathscr{A}(z)=0$ indicates that there exists only a single real positive root for each given value of a when $\tau<\tau_a$ or $\tau_b<\tau$. Consequently, the associated topological number and winding are both 1. For $\tau\in(\tau_a,\tau_b)$, the equation yields One negative root and three positive roots. The associated winding numbers are $w_1=1$, $w_2=-1$, and $w_3=1$, leading to a topological number $W=1$.

In this scenario, a BH exhibits one generation and one annihilation point, which categorizes the BH into small, intermediate, and large types based on the behavior of the vector field at zero points. This behavior highlights how the topological characteristics of the Kerr-AdS BH in PFDM differ from those of the Kerr BH in PFDM, where the topological number is $W=0$.

3.1.6 Impact of Electric Charge on the Kerr–Neumann BH in a Modified Context

Now, let us turn our attention to comprehending the significance of the electric charge for the topological numbers in thermodynamics. In PFDM, the action describing gravity theory with minimal coupling to the gauge field is given by, from which one can derive the spacetime geometry [78].

$$\mathscr{J} = \int dx^4 \sqrt{-g} \left(\frac{1}{16\pi G} R + \frac{1}{4} F^{\mu\nu} F_{\mu\nu} + \mathscr{L}_D M \right), \tag{3.75}$$

The last equation is

$$F_{\mu\nu} = \nabla_\mu A_\nu - \nabla_\nu A_\mu,$$

In the above, G represents the gravitational constant, R corresponds to the Ricci scalar, and the quantity $g = \det(g_{ab})$ represents the determinant of the metric tensor. The Lagrangian density for PFDM is denoted by $\mathscr{L}_{DM}$, and the electromagnetic field tensor is represented by $F_{\mu\nu}$. The field equations formulated by Einstein can be derived through the action principle's variation [78].

$$R_{\mu\nu} - \frac{1}{2} g_{\mu\nu} R = 8\pi G \left(T^M_{\mu\nu} + T^{DM}_{\mu\nu} \right), \tag{3.76}$$

Accompanied by

$$\begin{aligned} F^{\mu\nu}_{;\nu} &= 0, \\ F^{\mu\nu;\alpha} + F^{\nu\alpha;\nu} + F^{\alpha\mu;\nu} &= 0, \end{aligned} \tag{3.77}$$

The tensor $T^{DM}_{\mu\nu}$ represents the energy-momentum of ordinary matter, while $T^M_{\mu\nu}$ corresponds to the PFDM energy-momentum.

$$\begin{aligned} T^\mu_\nu &= g^{\mu\nu} T_{\nu\mu}, \\ T^t_t = -\rho, \quad T^r_r &= T^\theta_\theta = T^\phi_\phi = P, \end{aligned} \tag{3.78}$$

The line element of the dark matter background black hole that resembles a Kerr-Newman was demonstrated to be given as [78]

$$ds^2 = -\frac{\nabla}{\Sigma} \left(dt - a \sin^2\theta d\Phi \right)^2 + \frac{\Sigma}{\Delta} dr^2 + \Sigma d\theta^2 + \frac{\sin^2\theta}{\Sigma} \left[a dt - \left(r^2 + a^2 \right) d\phi \right]^2, \tag{3.79}$$

where

$$\begin{aligned} \Delta &= r^- 2mr + Q^2 + a^2 + ar \ln\left(\frac{r}{|\alpha|} \right), \\ \Sigma &= r^2 + a^2 \cos^2\theta, \end{aligned} \tag{3.80}$$

In this instance, Q represents the BH's electric charge. The horizon equation $\Delta = 0$ root analysis reveals that for any value of α, the metric element (4.81) represents a BH possessing three horizons. When the parameter a is associated with rotation, the charge Q satisfies the condition $a_2 + Q_2 < k_2$ and is a naked singularity otherwise. For this spacetime, the thermodynamic quantities are expressed as

$$M = m, \tag{3.81}$$

$$S = \pi \left(r^2 + a^2\right), \tag{3.82}$$

$$T = \frac{\Delta'(r_h)}{4\pi \left(r_h^2 + a^2\right)}, \tag{3.83}$$

The off-shell free energy for this BH is found to be as

$$\mathscr{F} = \frac{a^2 + \alpha r_h \ln\left(\frac{r}{|\alpha|}\right) + Q^2 + r_h^2}{2r_h} - \frac{\pi \left(a^2 + r_h^2\right)}{\tau}, \tag{3.84}$$

In this way, the n-vector field's components are given as

$$\phi^{rh} = \frac{1}{2r_h^2}\left(r_h^2 + \alpha r_h - a^2 - Q^2 - \frac{4\pi r_h^3}{\tau}\right), \tag{3.85}$$

$$\phi^{\theta} = -\cot\Theta \csc\Theta, \tag{3.86}$$

and

$$\tau = \frac{4\pi r_h^3}{r_h^2 + \alpha r_h - a^2 - Q^2}, \tag{3.87}$$

To determine the winding number, we specify

$$\mathscr{R}(z) = \frac{z^2 + \alpha z - a^2 - Q^2}{4\pi z^3 - \tau\left(z^2 + \alpha z - a^2 - Q^2\right)}, \tag{3.88}$$

Instead of $a_2 \to a_2 + Q_2$, it retains the same shape as the Kerr BH in PFDM [as given by Eq. (4.48)]. Given $a_2 + Q_2 < k$ and $\tau_c < \tau$, for any choice of α, an analogous analysis to that of the Kerr BH in Sect. 2 indicates that

$$\tau_c = 4\tau \frac{\left(-a + \sqrt{3\left(a^2 + Q^2\right) + a^2}\right)^3}{2a^2 - \alpha\left(-\alpha + \sqrt{3\left(a^2 + Q^2 + a^2\right)}\right)}, \tag{3.89}$$

For PFDM, the Kerr-Newman BH's winding number as well as the topological number, are

$$w_1 = -1 \quad , w_2 = 1, \quad W = 0, \tag{3.90}$$

3.1.7 The Reissner–Nordström BH in the context of PFDM

It possesses the metric element

$$ds^2 = -f(r)dt^2 + \frac{1}{f(r)}dr^2 + r^2\left(d\theta^2 + \sin^2\theta d\phi^2\right), \tag{3.91}$$

with

$$f(r) = 1 - \frac{2m}{r} + \frac{Q^2}{r^2} + \frac{\alpha}{r}\ln\left(\frac{r}{|\alpha|}\right), \tag{3.92}$$

In the case of $Q < k_c$ and $\tau < \tau_c$, the topological number as well as winding number of the Reissner-Nordström BH within the context of PFDM can be calculated in the same way as the Kerr-Newman BH.

$$w_1 = -1 \quad , w_2 = 1, \quad W = 0, \tag{3.93}$$

3.1.8 The influence of magnetic charge with nonlinear characteristics on the rotating Hayward BH under the influence of dark matter environment

The role that the magnetic charge plays will be examined in this section. Due to the coupling of Einstein's gravity with a nonlinear electromagnetic field accompanied by perfect fluid dark matter, one must begin with the action describing gravity theory with minimal coupling to the gauge field in the presence of PFDM to determine the spacetime geometry (Fig. 3.4). It is demonstrable that the following mathematical expressions take the form.

$$G_\mu^\nu = 2\left(\frac{\partial\mathscr{L}(F)}{\partial F}F_{\mu\nu}F^{\nu\lambda} - \delta_\mu^\nu\mathscr{L}\right) + 8\pi T_\nu^\mu(DM), \tag{3.94}$$

$$\nabla_\mu\left(\frac{\partial\mathscr{L}(F)}{\partial F}\right) = 0, \tag{3.95}$$

here $F_{\mu\nu} = 2\nabla_{[\mu}A_{\nu]}$ $\mathscr{L}$ is a function of $F \equiv \frac{1}{4}F_{\mu\nu}F^{\nu\lambda}$ it is given by [79]

$$\mathscr{L}(F) = \frac{3M}{|Q_m|^3}\frac{\left(2Q_m^2F\right)^{\frac{3}{2}}}{\left(1 + (2Q_m^2F)^{\frac{3}{2}}\right)^2}, \tag{3.96}$$

The revolving Hayward BH in the context of dark matter has a line element that is easily demonstrated to be [79].

$$ds^2 = -\frac{\Delta}{\Sigma}\left(dt - a\sin^2\theta d\phi\right)^2 + \frac{\Sigma}{\Delta}dr^2 + \Sigma d\theta^2 + \frac{\sin^2\theta}{\Sigma}\left[adt - \left(r^2 + a^2\right)d\phi\right]^2, \tag{3.97}$$

where

$$\Delta = r^2 - \frac{2mr^4}{r^3+Q_m^3} + a^2 + \alpha r \ln\left(\frac{r}{|\alpha|}\right),$$
$$\Sigma = r^2 + a^2\cos^2\theta, \tag{3.98}$$

In this case, Q is the black hole's electric charge. The BHs mass M, temperature T, entropy S, and magnetic charge Q_m are

$$M = m, \tag{3.99}$$

$$S = \pi\left[r_h^2 + a^2\frac{2Q_m^3}{r_h}\left(1+\frac{a^2}{3r_h^2}\right)\right], \tag{3.100}$$

$$T = \frac{\Delta'(t)}{4\pi\left(r_h^2+a^2\right)}|r_h, \tag{3.101}$$

We may determine the components of the n-vector field by applying the same technique as in the previous section.

$$\phi^{r_h} = \frac{1}{2\tau r_h^5}\left[r_h^3\left\{\tau\left(r_h^2+\alpha r_h - a^2\right) - 4\pi r_h^3\right\}\right.$$
$$\left. - Q_m^3\tau\left\{2r_h^2+4a^2+\alpha r_h\left(1-3\ln\left(\frac{r_h}{|\alpha|}\right)\right)+\frac{4\pi r_h}{\tau}\left(r_h^2+a^2\right)\right\}\right], \tag{3.102}$$

$$\phi^{\theta} = -\cot\Theta\csc\Theta, \tag{3.103}$$

Hence, the following is the inverse temperature parameter

$$\tau = 4\pi\frac{r_h^6 - Q_m^3 r_h\left(r_h^2+a^2\right)}{r_h^3\left(r_h^2+\alpha r_h - a^2\right) - Q_m^3\mathscr{H}(r_h)}, \tag{3.104}$$

where

$$\mathscr{H}(r_h) = 4a^2 + 2r_h^2 - \alpha r_h + 3\alpha r_h\ln\left(\frac{r}{|\alpha|}\right), \tag{3.105}$$

$\mathscr{R}(z)$, the complex function, has the following form

$$\mathscr{R}(z) \equiv -\frac{z^3\left(z^2+\alpha z - a^2\right) - Q_m^3\mathscr{H}(z)}{\mathscr{A}(z)}, \tag{3.106}$$

where

$$\mathscr{A}(z) = 4\pi\left\{z^6 + Q_m^3 z\left(z^2+a^2\right)\right\} - \tau\left\{z^3\left(z^2+\alpha z - a^2\right) - Q_m^3\mathscr{H}(z)\right\}, \tag{3.107}$$

Plotting $\mathscr{A}(z)$ for a rotating Hayward BH in PFDM [defined by Eq. (1.107) and shown in Fig. 8] allows us to analyze the complex function $\mathscr{R}(z)$ and, consequently, the winding number (Fig. 9). Two positive real solutions exist for the equation $\mathscr{A}(z)$, z_1 and z_2, with $z_1 < z_2$, as this figure illustrates. The related winding numbers are $w_1 = -1$ and $w_2 = 1$, with the topological number $W = 0$. Furthermore, we can observe that the revolving BH has a zero point or a 1 but no annihilation point, as shown in the graph of the zero point ϕ_h^r in Fig. 3.1.

3.1.9 Hayward BH in the Absence of PFDM: A Static Solution

The metric element corresponding to the Hayward BH is as follows in the absence of PFDM [79]

$$ds^2 = -f(r)dr^2 + \frac{1}{f(r)}dr^2 + r^2\left(d\theta^2 + \sin^2\theta d\phi^2\right), \tag{3.108}$$

where

$$f(r) = 1 - \frac{2mr^2}{r^3 + Q_m^3}, \tag{3.109}$$

In this instance, the zero point of the vector field, the radial component of the n vector, and the generalized off-shell free energy have the following form.

$$\mathscr{F} = \frac{1}{2r_h^2\tau}\left\{-2\pi r_h^4 + \tau r_h^3 + Q^3\left(\tau - 4\pi r_h\right)\right\}, \tag{3.110}$$

$$\phi^{r_h} = \frac{1}{2r_h^3\tau}\left\{\tau\left(r_h^3 - 2Q_m^3\right) - 4\pi r_h\left(r_h^3 + Q_m^3\right)\right\}, \tag{3.111}$$

$$\tau = \frac{4\pi r_h\left(r_h^3 + Q^3\right)}{r_h^3 - 2Q^3}, \tag{3.112}$$

The complex function is provided as follows to determine the winding numbers

$$\mathscr{R}_s(z) = -\frac{z^3 - 2Q^3}{4\pi z^4 - \tau z^3 + 4\tau Q^3 z + 2\tau Q^3} \equiv -\frac{z^3 - 2Q^3}{\mathscr{A}(z)}, \tag{3.113}$$

The expression of $\mathscr{A}(z)$ possesses two real positive roots for every value of Q and $\tau_c < \tau$, according to the root analysis of the function; In the lack of dark matter, these are the topological and winding numbers for the Hayward BH.

$$w_1 = -1, w_2 = 1 \quad and \quad W = 0, \tag{3.114}$$

which contrasts with those of the black hole Schwarschild. This demonstrates how winding and topological numbers are influenced by the magnetic charge Q_m in Hayward spacetime. The vector field n can be used to verify this in Fig. 3.1.

3.1.10 Hayward Black Hole within PFDM: A Static Approach

The metric element appears [79]

$$ds^2 = -f(r)dr^2 + \frac{1}{f(r)}dr^2 + r^2\left(d\theta^2 + \sin^2\theta d\phi^2\right), \tag{3.115}$$

Along with

$$f(r) = 1 - \frac{2mr^2}{r^3 + Q_m^3} + \frac{\alpha}{r}\ln\left(\frac{r}{|\alpha|}\right), \tag{3.116}$$

Here, Q_m is the charge of the magnetic monopole. The black hole's properties, including mass, entropy, and temperature associated with Hawking radiation, are given by

$$M = m, \tag{3.117}$$

$$S = \pi\left[r_h^2 - \frac{2Q_m^3}{r_h}\right], \tag{3.118}$$

$$T = \frac{f'(r)}{4\pi}|_{r_h}, \tag{3.119}$$

Such that

$$f(r) = 1 - \frac{2mr^2}{r^3 + Q_m^3} + \frac{\alpha}{r}\ln\left(\frac{r}{|\alpha|}\right), \tag{3.120}$$

The n vector field's radial components, zero point, and generalized off-shell free shell energy can be found as

$$\mathscr{F} = \frac{1}{2r_h^3\tau}\Big\{\left(r_h^3 + Q^3\right)\left(r_h + \alpha\ln\left(\frac{r}{|\alpha|}\right)\right) - \pi\left(r_h^3 - 2Q^3\right)\Big\}, \tag{3.121}$$

$$\begin{aligned}\phi^{r_h} = \frac{1}{2r_h^4\tau}\Bigg[& r_h^3\Big\{\tau\left(r_h^2 + \alpha r_h\right) - 4\pi r_h^3\Big\} \\ & - Q_m^2\tau\Big\{2r_h^2 + \alpha r_h\left(1 - 3\ln\left(\frac{r}{|\alpha|}\right) + \frac{4\pi r_h^3}{\tau}\right)\Big\}\Bigg],\end{aligned} \tag{3.122}$$

$$\tau = 4\pi\frac{r_h^3\left(r_h^3 + Q^3\right)}{r_h^3\left(r_h^2 + \alpha r_h\right) - Q_m^3\left(2r_h^2 - \alpha r_h + 3\alpha r_h\ln\left(\frac{r}{|\alpha|}\right)\right)}, \tag{3.123}$$

In this instance, the complex function is expressed as

$$\mathscr{R}(z) \equiv -\frac{z^3\left(z^3+\alpha z\right)-Q_m^3\left(2z^2-\alpha z+3\alpha z\ln\left(\frac{r}{|\alpha|}\right)\right)}{\mathscr{A}(z)}, \tag{3.124}$$

where

$$\mathscr{A}(z) = 4\pi z^3\left(z^3+Q_m^3\right)-\tau\Big\{z^3\left(z^2+\alpha z\right)-Q_m^3\left(2z^2-\alpha z+3\alpha z\ln\left(\frac{r}{|\alpha|}\right)\right)\Big\}, \tag{3.125}$$

We showed the function $\mathscr{A}(z)$ for the winding and topological number in Fig.9, which demonstrates that, for $\tau_c < \tau$, the Hayward BH under the influence of PFDM has three distinct positive real roots, in contrast to the Hayward BH and rotating variant under the influence of PFDM. Therefore, we can infer with ease that, like in earlier examples, the topological numbers and winding for the Hayward BH under the influence of PFDM are

$$w_1 = -1, w_2 = 1, w_3 = 1 \quad \textit{and} \quad W = 1, \tag{3.126}$$

Plotting of the vector field ϕ graph in Fig. 3.1 allows for the verification of this situation. Additionally, Figure 3.2 illustrates the zero point of ϕ, demonstrating that spacetime possesses both a generation and annihilation point.

3.1.11 Rotating Hayward BH

In this third specific instance, we will elaborate by including the effects of magnetic charge and rotation. In this instance, we obtain

$$\tau = 4\pi\frac{r_h^6+Q_m^3 r_h\left(r_h^2+a^2\right)}{r_h^3\left(r_h^2-a^2\right)-Q_m^3\left(4a^2+2r_h^2\right)}, \tag{3.127}$$

Conversely, the function R(z) has the following form

$$\mathscr{F} = -\frac{z^3\left(z^2-a^2\right)-Q_m^3\left(4a^2+2z^2\right)}{\mathscr{A}(z)}, \tag{3.128}$$

How we've established

$$\mathscr{A}(z) = 4\pi\Big\{z^6+Q_m^3\left(z^2+a^2\right)\Big\}-\tau\Big\{z^3\left(z^2-a^2\right)-Q_m^3\left(4a^2+2z^2\right)\Big\}, \tag{3.129}$$

Fig. 3.2 plots the function $\mathscr{A}(z)$ as a graph, demonstrating that $\mathscr{A}(z) = 0$ for $\tau_c < \tau$ has two positive real roots, resembling the Hayward black hole (Fig. 3.1), which has the same topological numbers and winding.

$$w_1 = -1, w_2 = 1, \quad \textit{and} \quad W = 0, \tag{3.130}$$

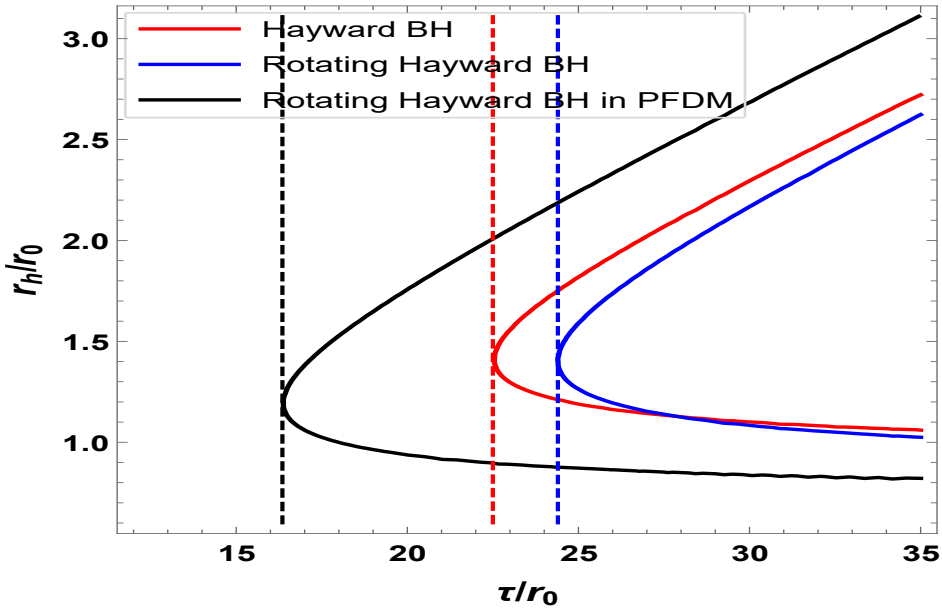

Figure 3.1: Plotting the zero point of ϕ for the BH class reveals that these BH have no annihilation point but just one generation point.

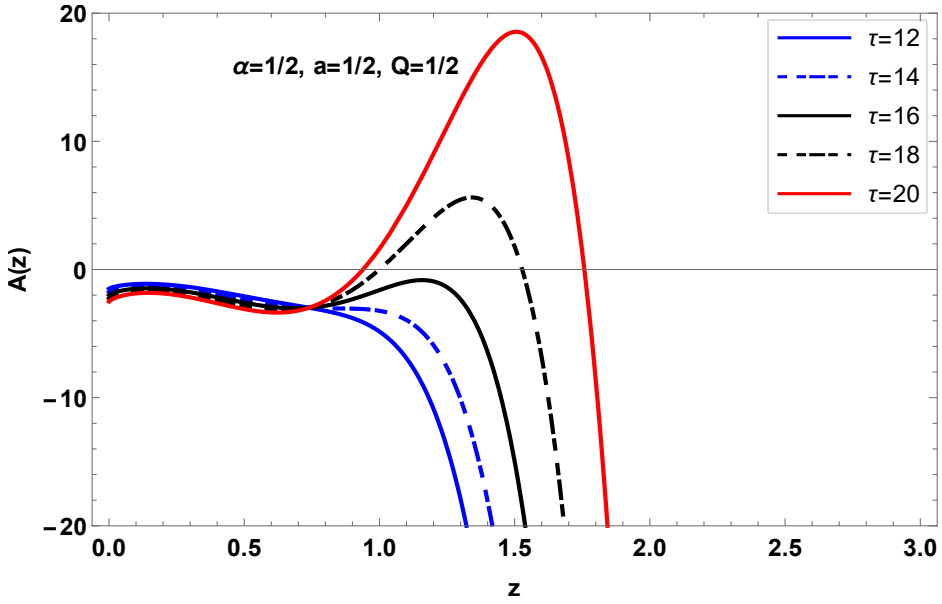

Figure 3.2: The graph of $A(z)$, plotted for different values of τ and mention vales of BH parameters.

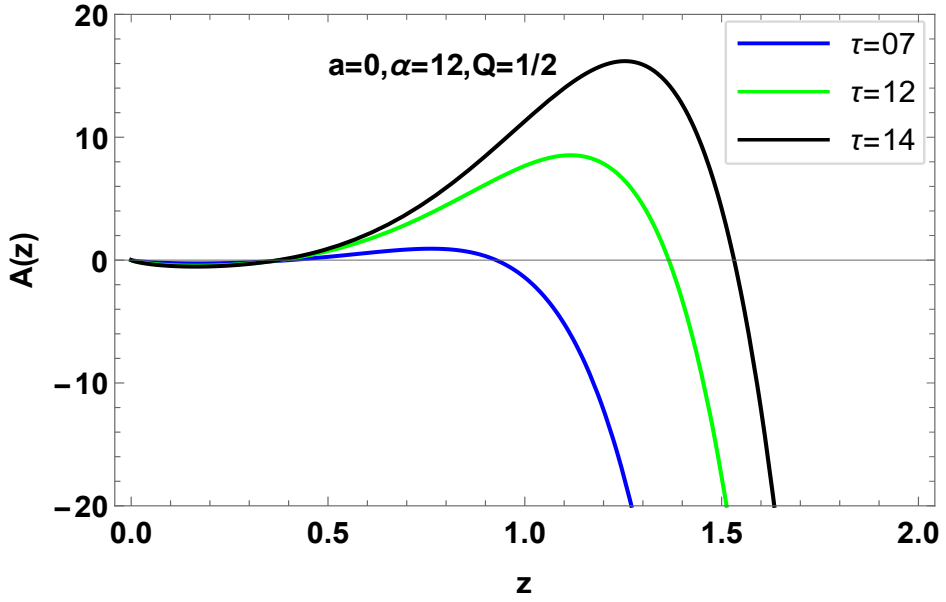

Figure 3.3: The graph of $A(z)$, plotted for different values of τ and mention vales of BH parameters.

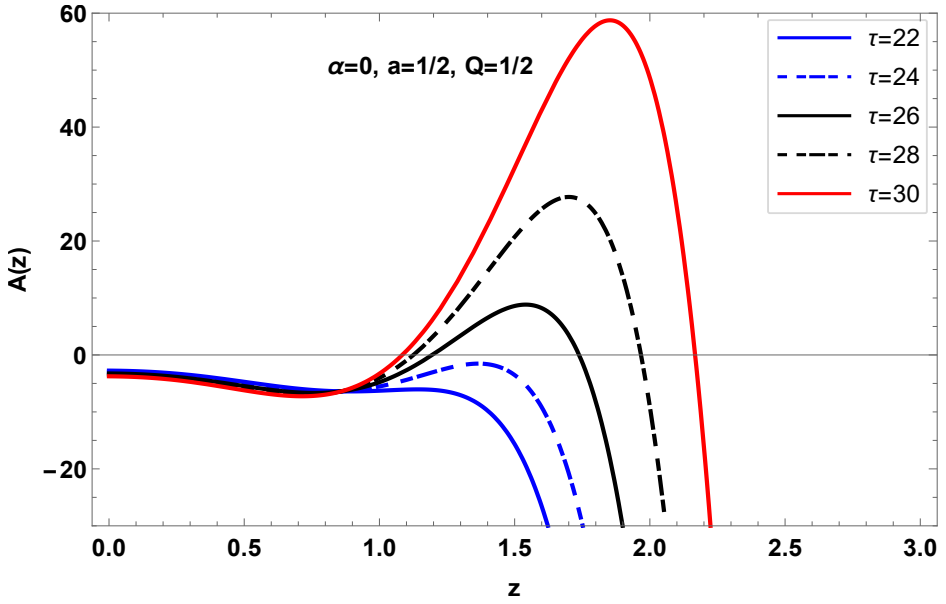

Figure 3.4: The function $A(z)$ [as defined by Eq. (100)] is graphed for several specified values of the rotating Hayward black hole without PFDM. The results indicate that when $\tau_c < \tau$, the equation $A(z) = 0$ results in two distinct positive roots.

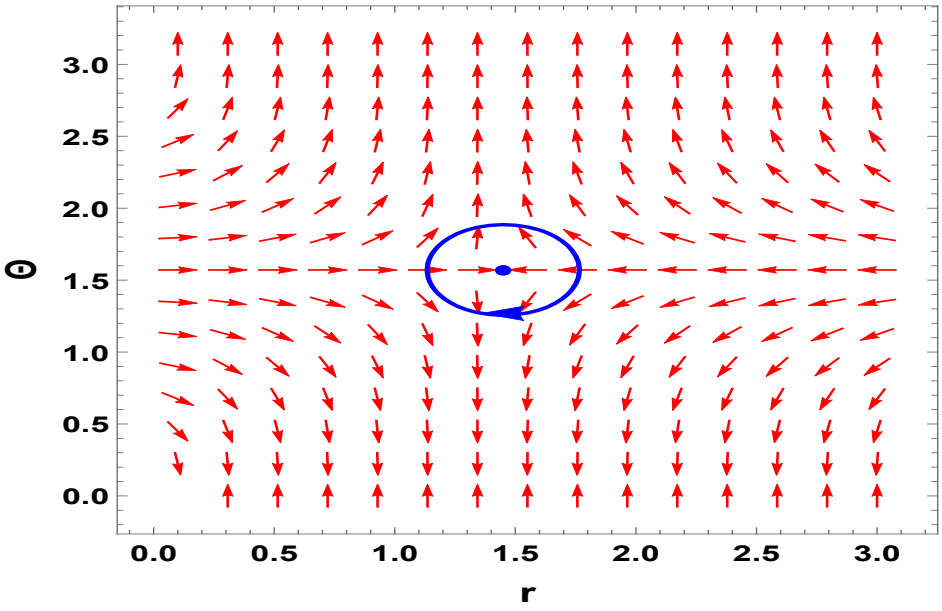

Figure 3.5: For $\tau/r_0 = 4\pi$ and $\alpha/r_0 = 1/2$, the zero points are indicated by blue dots. These points are located at $(r_h/r_0, \theta) = (0.35, \frac{\pi}{2})$ and $(1.24, \frac{\pi}{2})$ on the left-hand side, as well as $(r_h/r_0, \theta) = (1.37, \frac{\pi}{2})$ on the right-hand side.

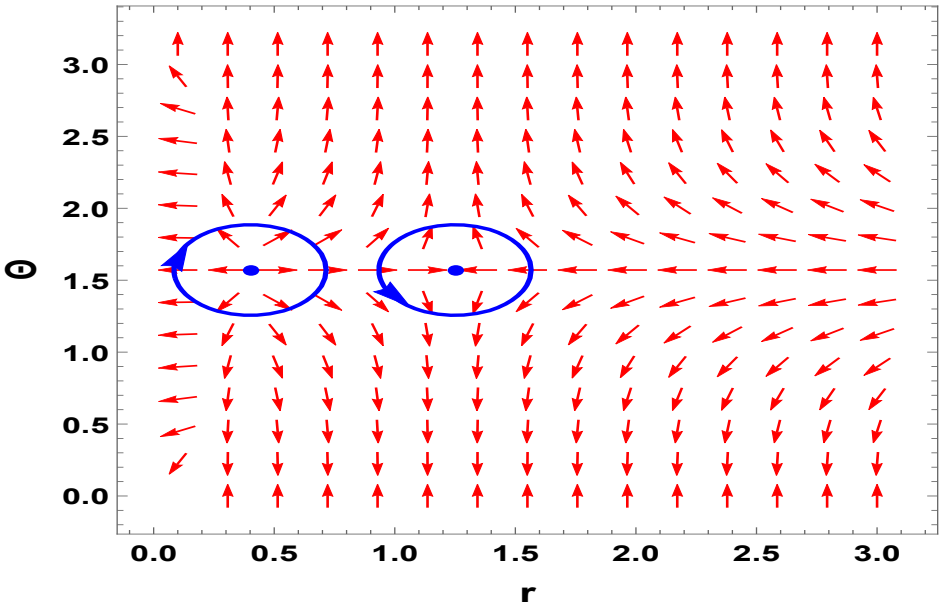

Figure 3.6: The red arrows indicate the unit vector field with parameters for Kerr BH in PFDM $a/r_0 = \frac{1}{2}$, $\tau/r_0 = 4\pi$, and $\alpha_0 = \frac{1}{2}$.

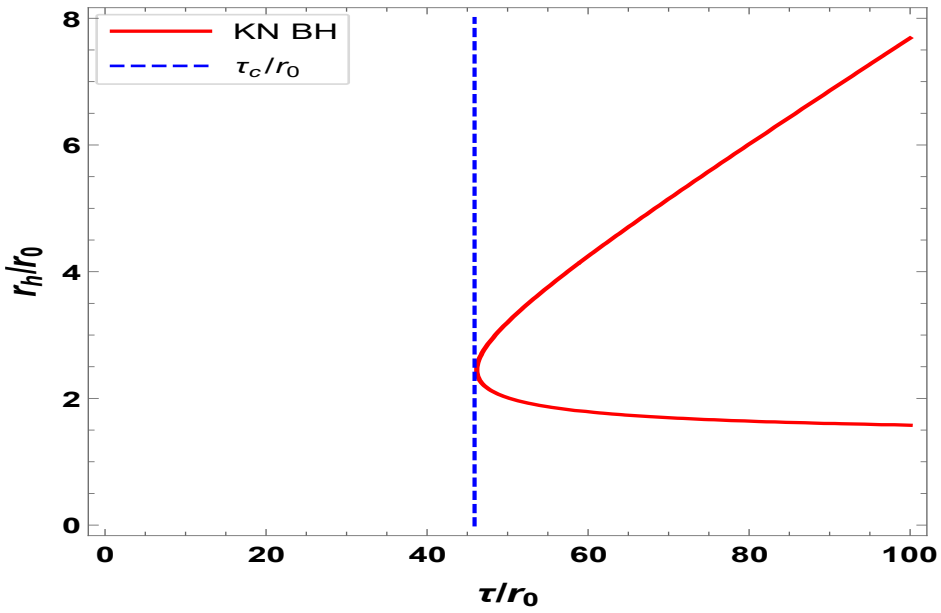

Figure 3.7: The ZPs of the vector ϕ^{r_h} for the Kerr-Newman BH are displayed with these parameters: $a/r_0 = 1$ and $Q/r_0 = 1$.

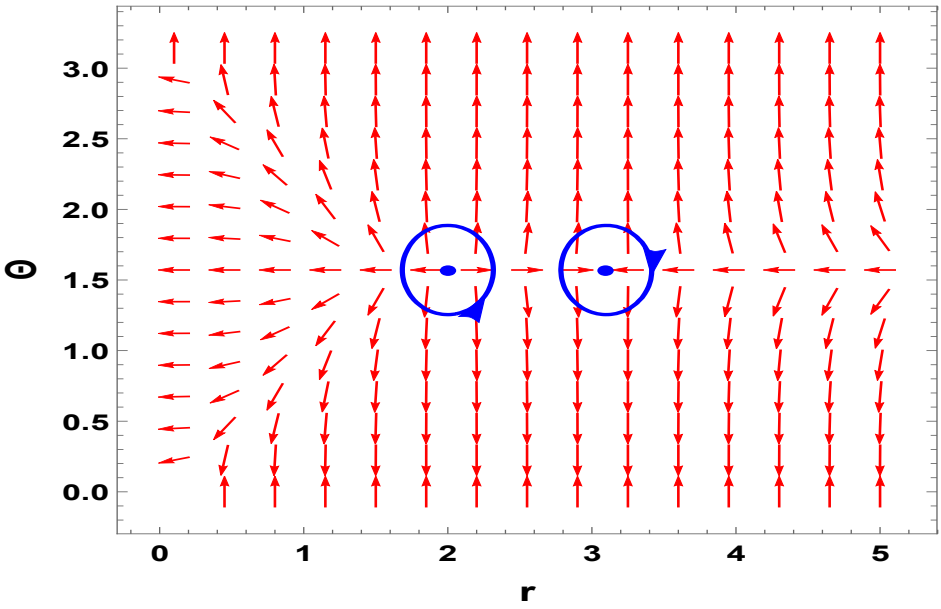

Figure 3.8: This vector field is shown for the Kerr-Newman BH with $r_0 = 50$, $a/r_0 = 1$, and $Q/r_0 = 1$. The zero points (ZPs), indicated by blue dots, are positioned at $(r_h/r_0, \Theta) = (1.95, \pi/2)$ for ZP_1 and $(3, \pi/2)$ for ZP_2.

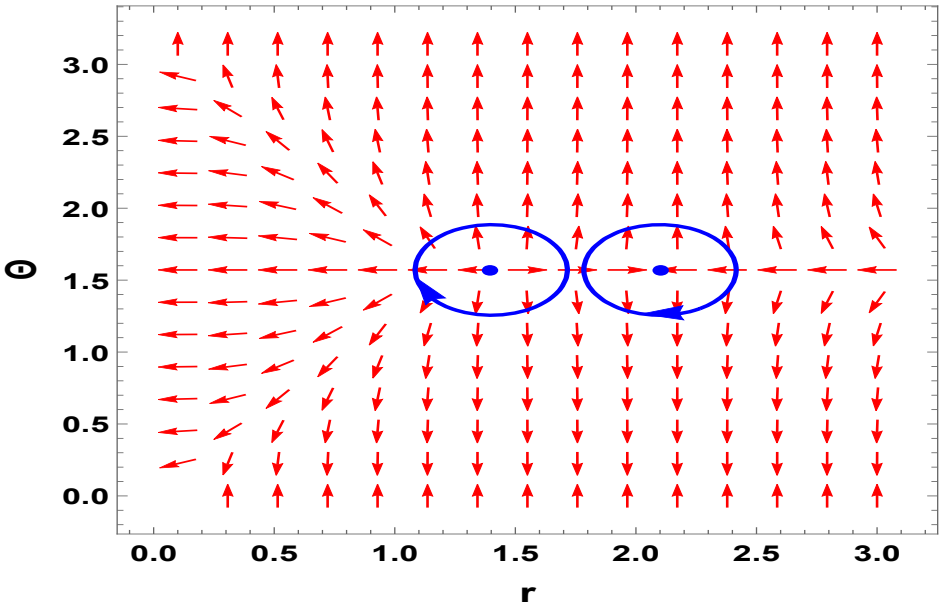

Figure 3.9: (a) This vector field is shown for the Kerr-Newman BH with $r_0 = 50$, $a/r_0 = 1$, and $Q/r_0 = 1$. The zero points, indicated by black dots, are positioned at $(r_h/r_0, \Theta) = (1.95, \pi/2)$ for ZP_1 and $(3, \pi/2)$ for ZP_2.

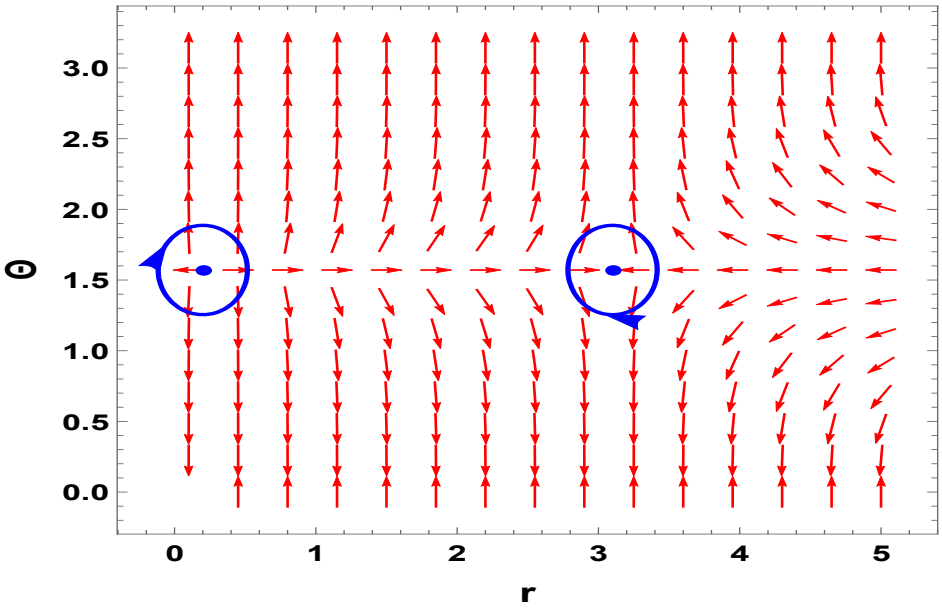

Figure 3.10: This vector field is shown for the Kerr BH with $\tau/r_0 = 20$, $a/r_0 = 1$. The zero points (ZPs), indicated by blue dots, are positioned at $(r_h/r_0, \Theta) = (0.29, \pi/2)$ for ZP_1 and $(3.15.16, \pi/2)$ for ZP_2.

Black Hole	**W**	**GP**	**AP**
Schwarzschild BH	-1	0	0
Schwarzschild BH in PFDM	-1	0	0

Table 3.1: Values of W, GP, and AP.

Black Hole	**W**	**GP**	**AP**
Schwarzschild-AdS_4 BH	0	0	1
Reissner-Nordström BH	0	1	0
Kerr BH	0	1	0
Kerr-Newman BH	0	1	0
Kerr-Newman BH in PFDM	0	1	0
Reissner-Nordström BH in PFDM	0	1	0
Hayward BH	0	1	0
Rotating Hayward BH	0	1	0
Hayward BH in PFDM	0	1 or 0	1 or 0
Rotating Hayward BH in PFDM	0	1	0

Table 3.2: Values of W, GP, and AP.

Black Hole	**W**	**GP**	**AP**
Reissner-Nordström ADS_4 BH	1	1 or 0	1 or 0
AdS Kerr BH	1	1 or 0	1 or 0
Kerr-Newman AdS_4 BH	1	0	0
AdS Kerr BH in PFDM	1	1 or 0	1 or 0

Table 3.3: Values of W, GP, and AP.

CHAPTER 4

TOPOLOGICAL CLASSES OF BLACK HOLES IN DARK ENERGY BACKGROUND

4.1 Introduction

In this chapter, we will examine the thermodynamical topological classes of rotating BH in a dark energy background. In the literature, it was conjectured that all BHs can be classified into three thermodynamical topological classes with topological numbers $-1, 0, 1$ [5]. We will test this conjecture for various BHs in a dark energy background, including the Kiselev BH (an extension of the Schwarzschild BH), the rotating Kiselev BH (an extension of the Kerr BH), and the charged rotating BH in dark energy (an extension of the Kerr-Newman BH). Our analysis will focus on how the dark energy parameter and the rotation parameter influence the topological number in different configurations. The study of how dark energy interacts with BH thermodynamics is important because it helps us understand both the universe's large-scale structure (cosmology) and the strange world of quantum gravity. By looking at how charge and rotation affect these BHs, we might find deeper connections between the physical laws that govern large objects and tiny particles. This research contributes to the advancing understanding of BHs and explores concepts such as the behavior of spacetime near singularities and the fundamental nature of these extreme environments.

4.2 Kiselev BH

To analyze the thermodynamical topological classes of the Kiselev BH, we begin by considering its line element and thermodynamical quantities. Understanding these classes provides insight into how dark energy influences the thermodynamic behavior of spacetime, focusing solely on the mass of the BH as the primary parameter. The Kiselev black hole has been widely explored in the literature within different contexts, and its line element is detailed in the foundational work by Kiselev [24]

$$ds^2 = -f(r)dt^2 + \frac{1}{f(r)}dr^2 + r^2 d\Omega^2, \tag{4.1}$$

where $d\Omega^2 = d\theta^2 + \sin^2\theta d\pi^2$ is the angular part of the metric, and

$$f(r) = 1 - \frac{2m}{r} - \frac{c}{r^{1+3\omega}}, \tag{4.2}$$

M is the BHs central mass, which determines its gravitational pull's strength. c represents how strong the influence of the quintessence field is around the BH. Quintessence is a hypothetical form of dark energy that affects spacetime geometry .ω characterizes the correlation between the pressure (p) and energy density (ρ) of the quintessence field. The thermodynamic characteristics of the Schwarzschild BH within a dark energy context are presented as follows

$$M = m, \quad S = \pi r_h^2, \tag{4.3}$$

When the dark energy background is not considered for c=0 the thermodynamic quantities and line element reduce to that of Sch BHs. For the Kiseleve BH in a dark energy background, the form of the generalized off-shell free energy is expressed as

$$\mathscr{F} = \frac{1}{2} r_h^{1-3\omega}\left(-c + r_h^{1+3\omega}\right) - \frac{\pi r_h^2}{\tau}, \tag{4.4}$$

So, the vector field components are

$$\phi^{r_h} = \frac{1}{2} + \frac{3}{2} c r_h^{-1-\omega}\omega - \frac{2\pi r_h}{\tau}, \tag{4.5}$$

$$\phi^{\theta} = -\cot\theta \csc\theta, \tag{4.6}$$

which gives the value of τ that is inverse of temperature parameter

$$\tau = \frac{4\pi r_h^{2+3\omega}}{r_h^{1+3\omega} + 3c\omega}, \tag{4.7}$$

This indicates that as the dark matter parameter c increases, the inverse of the temperature parameter τ decreases. Additionally, when $c = 0$, the result corresponds to that of the Sch BH.The equation has no real roots when $\omega = -2/3$. This result suggests that the expression inside the parentheses,$-3.0c\omega\,(3.0\omega + 2.0)$, either leads to an undefined result or produces a complex value for r under the given conditions. Specifically, with $\omega = -2/3$, the expression might not be valid for real values of r, causing no real roots to exist for this configuration. It becomes challenging to compute the winding number directly from the standard way. It's crucial to examine the equation's behavior close to the singularities and critical points if it lacks real roots. The winding number can still be investigated by looking at numerical simulations or approximations or examining how the solution behaves in the complex plane. The analysis of the contour plot for different values of c yields the related winding number (w_1) and topological number are expressed as follows

$$w_1 = -1, \quad and \quad W = -1. \tag{4.8}$$

From panel (a) of Fig. 4.1 In $r_h - \tau$ plane the point where the vector ϕ^{rh} equals zero also shows that winding and topological number for Kiselev BH within the dark energy background align with Kiselev BH.

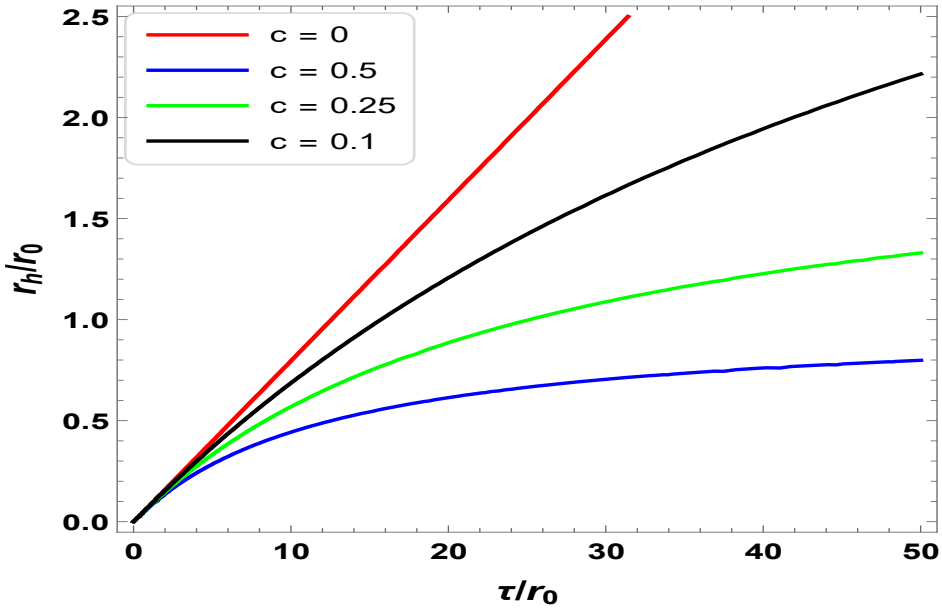

(a) In $r_h - \tau$ plane the point where the vector ϕ^{rh} equals zero also shows a winding number for Kiselev BH within the dark energy background aligned with Kiselev BH. The red, black, yellow, and blue solid lines are for different values of c with $\omega = -2/3$

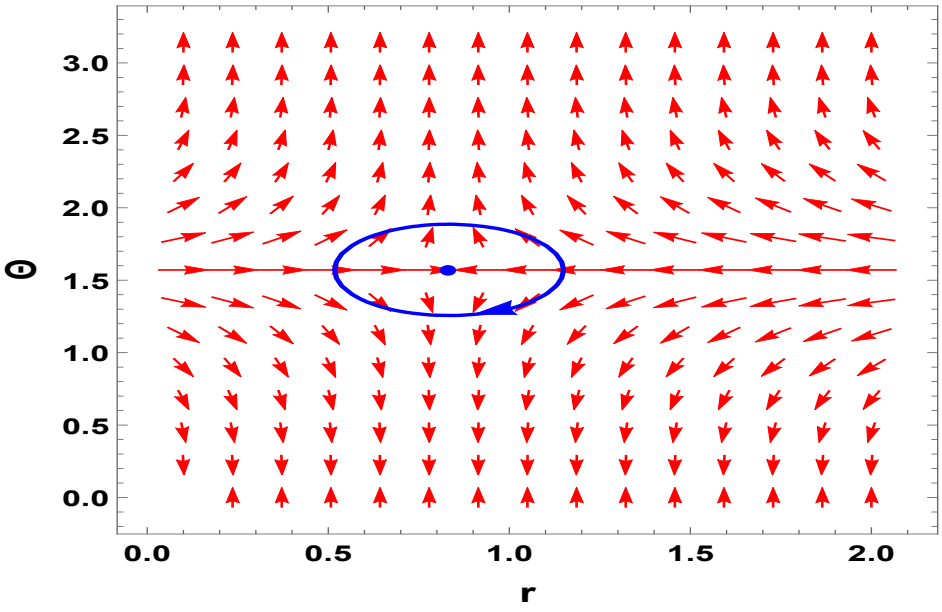

(b) Unit vector field is plotted for the Kiselev BH with $\tau/r_0 = 4\pi$ and $c = 0.1$. The zero point highlighted by blue dots are at $(r_h/r_0, \Theta) = (0.83, \pi/2)$ for ZP_1.

Figure 4.1: Graphs of Kiselev BH when $\omega = -2/3$

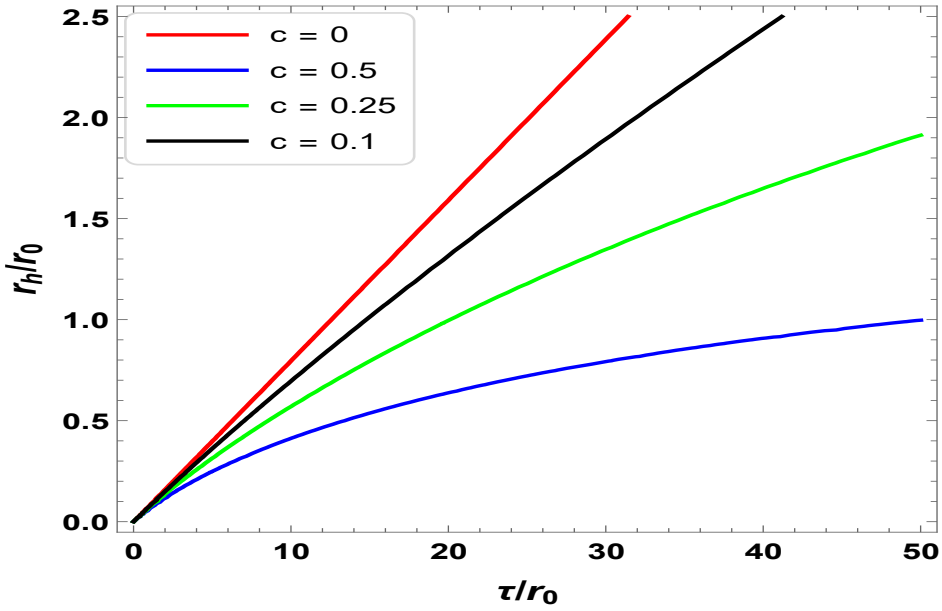

(a) The red, black, yellow, and blue solid lines are for different values of c with $\omega = -1/2$.

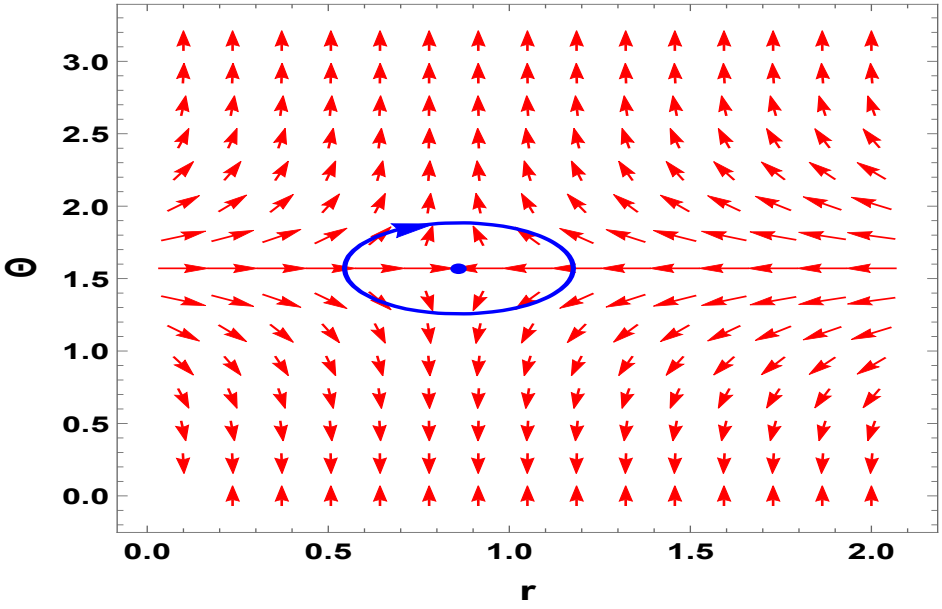

(b) Unit vector field is plotted for the Kiselev BH with $\tau/r_0 = 4\pi$ and $c = 0.1$. The zero point (ZPs) highlighted by blue dots are at $(r_h/r_0, \Theta) = (0.86, \pi/2)$ for ZP_1.

Figure 4.2: Graphs of kiselev BH when $\omega = -1/2$

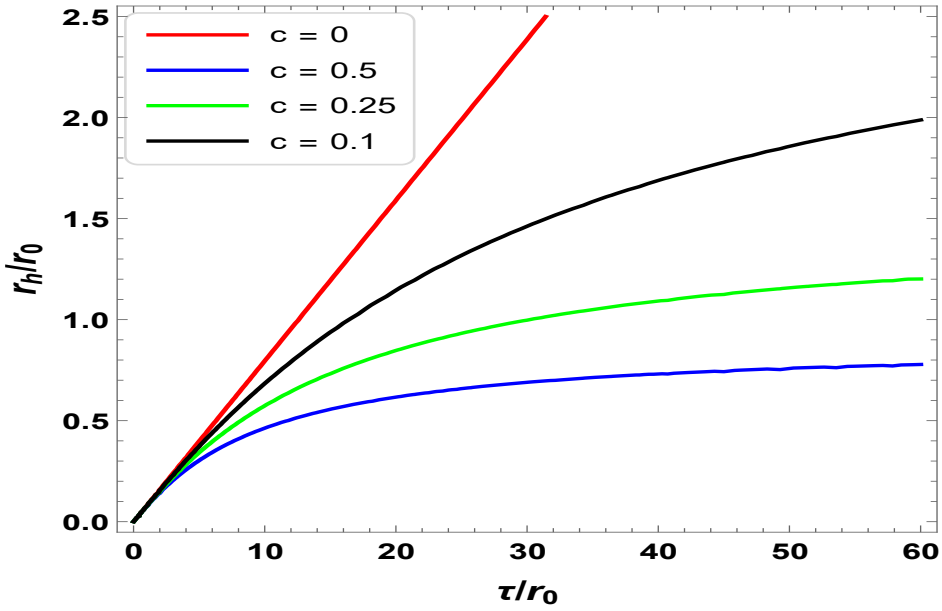

(a) The red, black, yellow, and blue solid lines are for different values of c with $\omega = -7/9$.

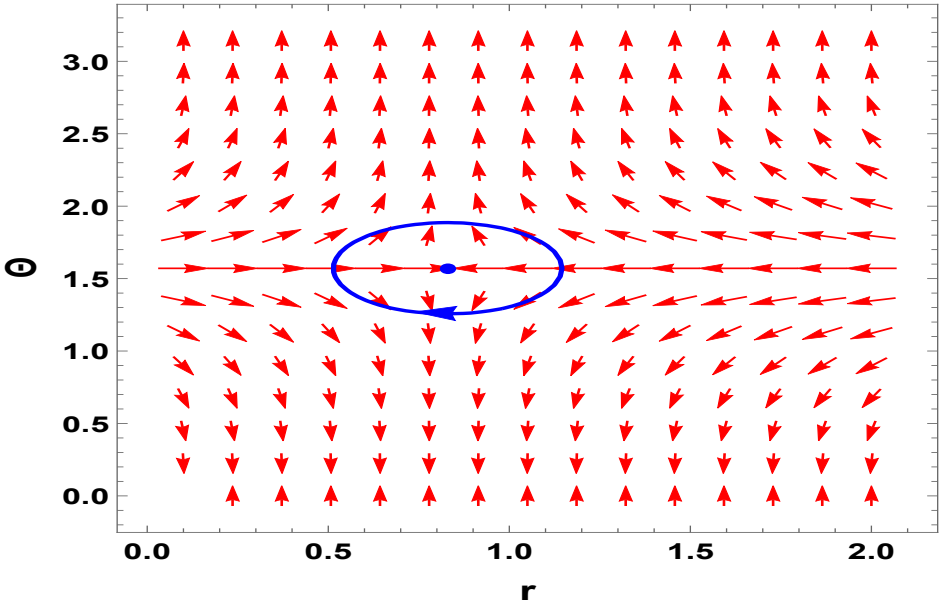

(b) it is plotted for the Kiselev BH with $\tau/r_0 = 4\pi$ and $c = 0.1$ The zero point highlighted by blue dots are at $(r_h/r_0, \Theta) = (0.83, \pi/2)$ for ZP_1.

Figure 4.3: Graphs of kiselev BH when $\omega = -7/9$

4.2.1 Rotating Kiselev Quintessential BH

Now, we will calculate the topological number associated with a quintessential BH. To do this, we start by considering a quintessential BH, a theoretical type of BH influenced by quintessential matter(a hypothetical form of dark energy). The line element, or the metric of spacetime around this BH, can be expressed in a way that captures how quintessential matter affects the curvature of spacetime. By analyzing this line element, we can determine the BH's topological properties, which are essential for understanding its unique structure and behavior in a universe with dark energy. The lie element can be expressed as [80]

$$ds^2 = -\left(1-\frac{2Mr+cr^{1-3\omega}}{\Sigma}\right)dt^2+\frac{\Sigma}{\Delta}dr^2-2a\sin^2\theta\left(\frac{2Mr+cr^{1-3\omega}}{\Sigma}\right)d\phi dt \qquad (4.9)$$
$$+\Sigma d\theta^2+\sin^2\theta\left[r^2+a^2+a^2 sin^2\theta\left(\frac{2Mr+cr^{1-3\omega}}{\Sigma}\right)\right]d\phi^2,$$

where

$$\Delta = r^2-2Mr+a^2-cr^{1-3w}, \qquad (4.10)$$

where m denotes mass and a denotes the spinning parameters.To evaluate the thermodynamic spacetime defined by (1) are as follows,

$$M=\frac{a^2+r^2-cr^{1-\omega}}{2r}, \quad S=\pi\left(r_h^2+a^2\right), \qquad (4.11)$$

The generalized off-shell free energy can be introduced first in the context of BHs. This allows us to investigate BH energy landscapes outside of their usual equilibrium states.

$$\mathscr{F}=M-\frac{S}{\tau}, \qquad (4.12)$$

where M is mass S is entropy and τ is an extra variable that is equal to the inverse of temperature. In Ref.[10] a vector ϕ define as,

$$\phi=\left(\frac{\partial\mathscr{F}}{\partial r_+}\ ,-\csc\theta\ \cot\theta\right), \qquad (4.13)$$

The generalized free energy can be readily obtained from the data previously provided in equation (5.11).

$$\mathscr{F}=\frac{a^2+r_h^2-cr_h^{1-\omega}}{2r_h}, \qquad (4.14)$$

Consequently, the vector ϕ components can be evaluated as

$$\phi^{r_h} = \frac{1}{2} + \frac{a^2}{2r_h^2} + \frac{1}{2}(1-b)\,c r_h^{b-2} + \frac{2\pi r_h}{\tau}, \tag{4.15}$$

$$\phi^{\Theta} = -\cot\Theta \csc\Theta, \tag{4.16}$$

when we evaluate the above eqcation for $\phi^{r_h} = 0$. we get the expression for component τ.

$$\tau = \frac{4\pi r_h^3}{-a^2 + r_h^2 + c r_h^b - b c r_h^b}, \tag{4.17}$$

The critical values of the inverse Hawking temperature parameter, τ, depend on the choice of ω. For general values of ω within the range $-1 < \omega < -1/3$, determining these values explicitly is challenging because a general ω produces algebraic equations in non-polynomial form. Therefore, we focus on specific cases to proceed with the analysis. The first case, $\omega = -2/3$, where the equation for extreme values simplifies to a polynomial form, has been extensively studied in the literature [81].

4.2.2 When $\omega = -2/3$

In this instance, we concentrate on the Kiselev BH's topological and thermal characteristics for $\omega = -2/3$. The calculations highlight a significant phase transition in the system, which shows a critical value of τ_c, the inverse temperature parameter. To find the value of τ_c, the critical radius was solved and then substituted into the inverse temperature formula. This critical value is a key indicator of the system's behavior and transition points. The link between the inverse temperature and the normalized horizon radius can be seen in detail through a graphical analysis using contour plots for different values of the parameter c. The plot of the evolution of the thermal properties of the BH with variations in c provides important information on the stability and structure of the rotating Kiselev BH. Furthermore, the comprehension of system stability is reinforced by vector field analysis. The flow lines of the polar coordinate representation better comprehend the dynamics under $\omega = -2/3$ by showing the critical points and their stability features. This analysis clarifies the peculiar behavior of the Kiselev BH in this particular instance by highlighting the complex interactions between its parameters and its topological and thermal characteristics.

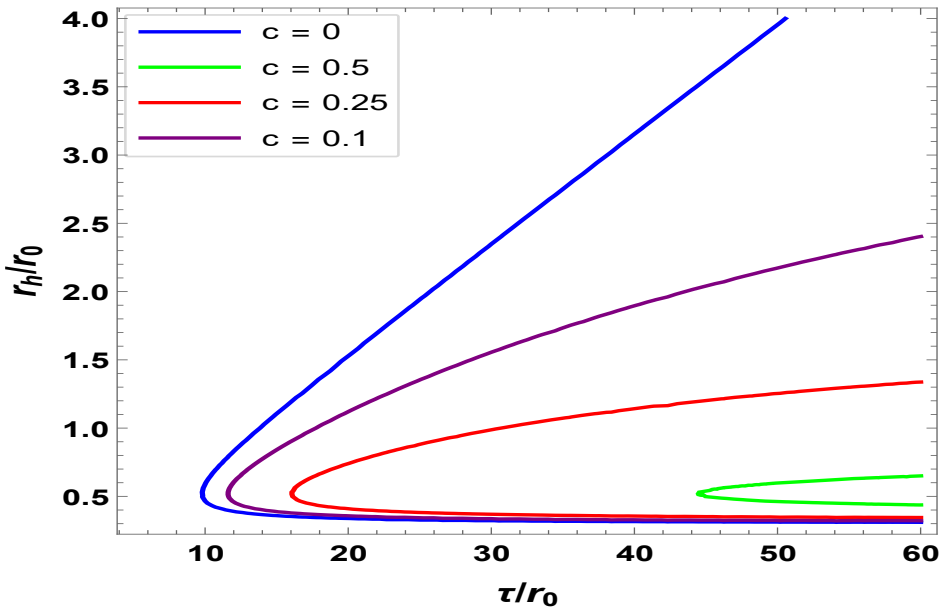

(a) In $r_h - \tau$ plane the point where the vector ϕ^{rh} equals zero also shows a winding number for rotating Kiselev BH within the dark energy background with $\omega = -2/3$ and $a/r_0 = 0.4$. τ_c serves as a generation point for different values of c. The value of τ_c splits the rotating Kiselev BH into two distinct branches: upper and lower, characterized by the winding numbers. It is observed that the topological number W is zero.

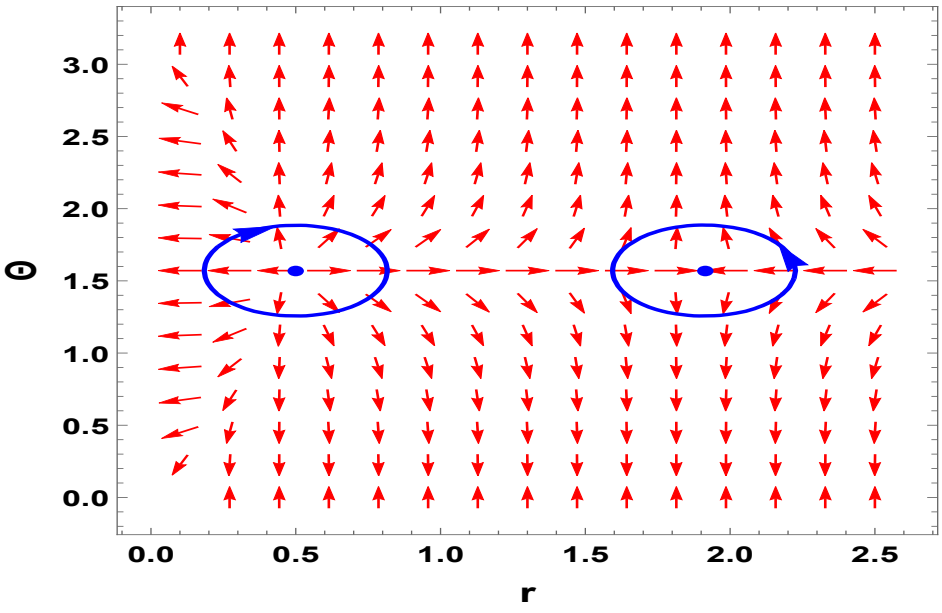

(b) it is plotted for the rotating Kiselev BH with $\tau/r_0 = 40$ and $c = 0.1$. The zero points (ZP_1) and ZP_2 highlighted by blue dots are at $(r_h/r_0, \Theta) = (0.5, \pi/2)$ and $(1.91, \pi/2)$ for ZP_1, and ZP_2 respectively.

Figure 4.4: Graph of rotating kiselev BH when $\omega = -2/3$

4.2.3 When $\omega = -1/2$

The analysis shows the Kiselev BH's interesting topological and thermal features when $\omega = -1/2$. In contrast to other values of ω, the contour lines in this case's graph exhibit minor fluctuations; however, the winding number and topological number remain consistent. Accordingly, the basic topological properties of the BH remain unchanged, even in the presence of slight variations in the temperature profile. While the vector field analysis verifies the stability of the critical points, the contour plot emphasizes the delicate effect of parameter c on the inverse temperature instead. Despite slight variations in its thermal properties, the BH retains its topological structure in the balanced situation of $\omega = -1/2$, as these observations confirm.

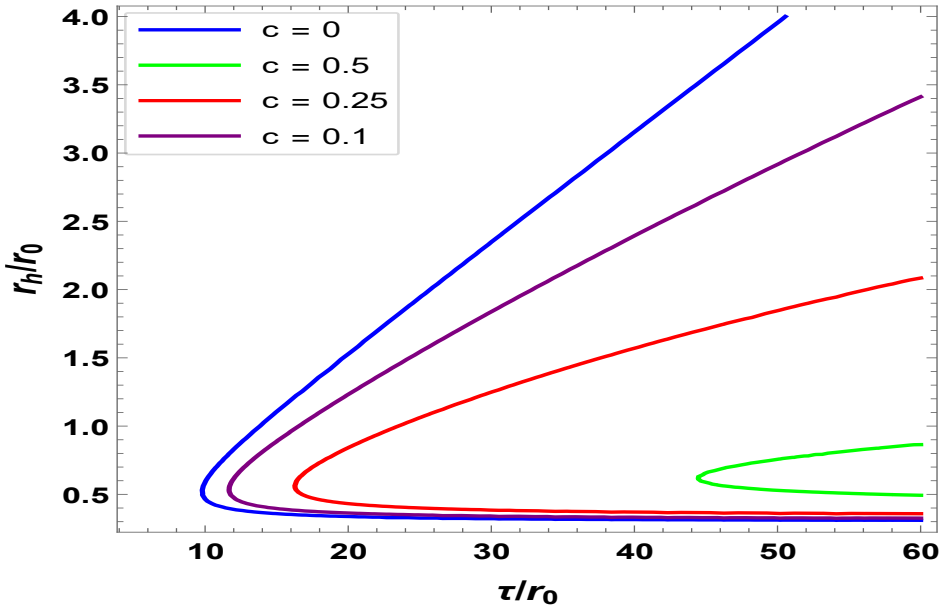

(a) when $\omega = -1/2$ and $a/r_0 = 0.4$. the value τ_c serves as a generation point for different values of c.

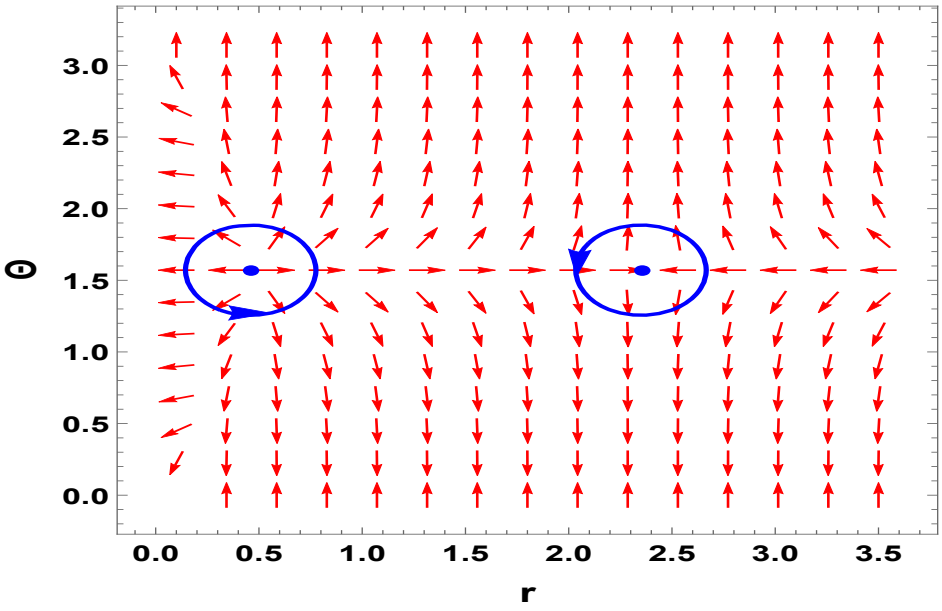

(b) it is plotted for the rotating Kiselev BH with $\tau/r_0 = 40$ and $c = 0.1$ The zero points (ZPs) and ZP_2 highlighted by blue dots are at $(r_h/r_0, \Theta) = (2.35, \pi/2)$ and $(0.46, \pi/2)$ for ZP_1, and ZP_2 respectively.

Figure 4.5: Graph of rotating Kiselev BH when $\omega = -1/2$

4.2.4 When $\omega = -7/9$

For the interval $-1 < \omega < -1/3$, taking $\omega = -7/9$ shows that the critical radius (r_c) and the critical inverse temperature (τ_c) change compared to other values of ω .We obtain the same results as when $\omega = -2/3$ and $\omega = -1/2$, where modifications in the geometric and thermal qualities do not affect the topological number or winding number. This shows that the underlying topology of the Kiselev BH remains stable throughout this timescale. Confirmed by contour and vector plots, the results show that the BH's core topological properties remain stable even at $\omega = -7/9$.

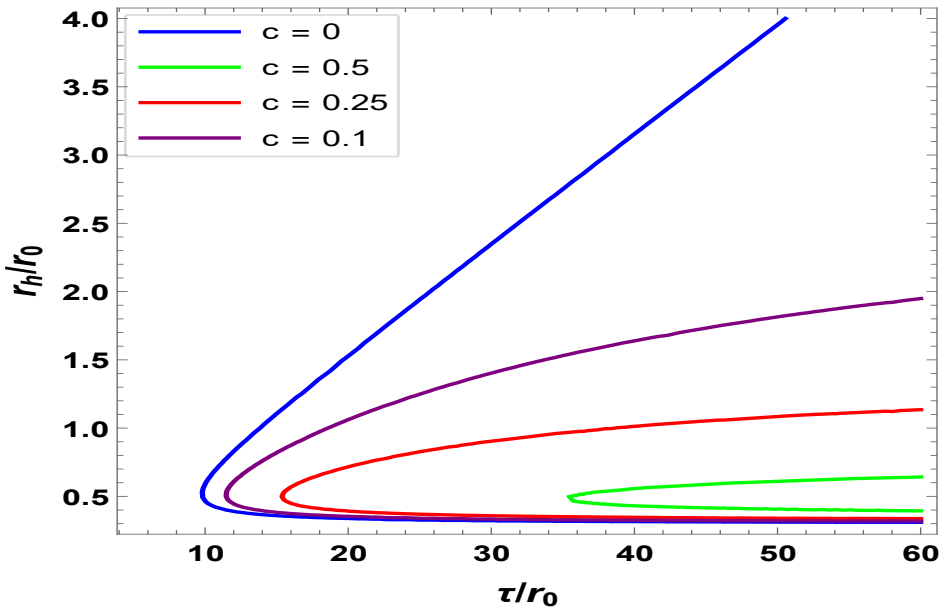

(a) when $\omega = -7/9$ and $a/r_0 = 0.4$. the value τ_c serves as a generation point for different values of c.

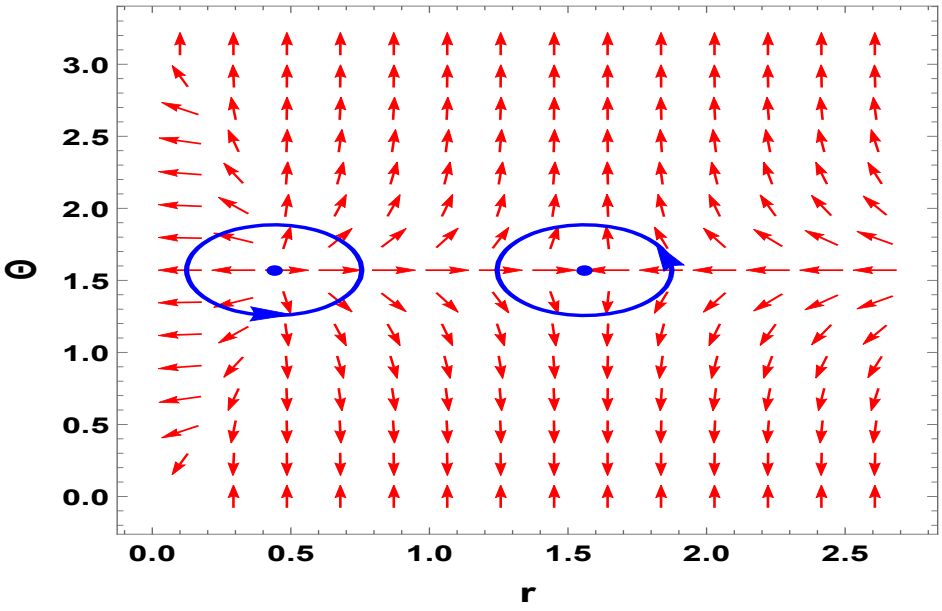

(b) it is plotted for the rotating Kiselev BH with $a = 0.4$ $\tau/r_0 = 40$ and $c = 0.1$ The zero points ZP_1 and ZP_2 highlighted by blue dots are at $(r_h/r_0, \Theta) = (1.56, \pi/2)$ and $(0.44, \pi/2)$ for ZP_1, and ZP_2 respectively.

Figure 4.6: Graph of rotating Kiselev BH when $\omega = -7/9$

From the above discussion when we consider $\omega = -2/3$ in Fig 4.1 shows that The zero points of the component ϕ^{r_h} for rotating kiselev BH correspond to $a = r_0$, where r_0 represents

an arbitrary length scale defined by the cavity enclosing the BH. For large τ, such as $\tau = \tau_2$, two intersections can be identified for the rotating kiseleve BH, respectively. The intersection points precisely satisfy the condition $\tau = 1/T$ thereby representing off-shell BH solutions characterized by a temperature $T = 1/\tau$. These solutions highlight the relationship between the inverse temperature and the parameter τ in defining BH thermodynamics. The two intersection points for the rotating Kiseleve BH they become identical when $\tau = \tau_c$, and then vanish when $\tau < \tau_c$.Especially, at the point $\tau_c = \frac{6\sqrt{3}\pi}{a(1-3\sqrt{3}ac)^2}$, One can easily find a solution for the rotating Kiselev BH. This suggests that τ_c serves as a generation point, which is also evident from Fig 4.4. Moreover, the generation point splits rotating Kiselev BH into upper and lower branches, characterized by the winding numbers . As a result, the topological number for the rotating Kiselev BH is determined to be $W = 0$.

As an alternative, the unit vector field n can be plotted for a range of randomly selected typical values to calculate the topological number for the rotating Kiselev BH. it is important to note that τ must be greater than τ_c. For example, $\tau/r_0 = 40$ and $a/r_0 = 0.4$ in Fig 4.4 where we find two zero points: ZP_1 at $r_h = 0.5$ and ZP_2 at $r_h = 1.91$ with the winding numbers $w_1 = -1$,$w_2 = 1$, respectively . So one can get the topological number $W = w_1 + w_2 = 0$ for the rotating kiselev BH. The topological number of the rotating Kiselev BH is zero, according to the classifying proposal for BH solutions, which is based on its distinct topological numbers [5]. An uncharged BHs topological number is greatly influenced by the rotation parameter, as evidenced by the rotating Kiselev BH's topological number of 0 and the Schwarzschild BHs topological number of -1.

4.3 Kerr-Newman Quintessential BH

We start by looking at the line element and thermodynamic quantities of the Kerr-Newman quintessential BH to examine its thermodynamic topological classes. The line element of a charged spinning BH surrounded by quintessence is given by the following expression [82].

$$ds^2 = -\frac{\Delta - a^2\sin^2\theta}{\Sigma}dt^2 + \frac{\Sigma}{\Delta}dr^2 + 2a\sin^2\theta\left(1 - \frac{\Delta - a^2\sin^2\theta}{\Sigma}\right)dtd\phi + \Sigma d\theta^2 \quad (4.18)$$
$$+ \sin^2\theta\left[\Sigma + a^2\sin^2\theta\left(2 - \frac{\Delta - a^2\sin^2\theta}{\Sigma}\right)\right]d\phi^2,$$

Here, a represents the BHs angular momentum per unit mass, and

$$\Delta = r^2 + a^2 + Q^2 - 2Mr - cr^{1-3\omega}, \tag{4.19}$$

In this context, Q denotes the electric charge of the black hole. Analyzing the roots of the horizon equation $\Delta = 0$ helps determine whether the solution describes a black hole or a naked singularity.

The thermodynamic properties associated with this spacetime are expressed as follows

$$M = m, \tag{4.20}$$

$$S = \pi\left(r_h^2 + a^2\right), \tag{4.21}$$

$$T = \frac{r_h^2 - a^2 - Q^2 + 3\omega_q r^{1-3\omega}}{4\pi r_h\left(r_h^2 + a^2\right)}, \tag{4.22}$$

By utilizing these thermodynamic quantities, the generalized off-shell free energy of the system can be derived as

$$\mathscr{F} = \frac{a^2 + Q^2 + r_h^2 - cr_h^b}{2r_h} - \frac{\pi(r_h^2 + a^2)}{\tau}, \tag{4.23}$$

As a result, the components of the vector field can be expressed as

$$\phi^{r_h} = \frac{1}{2} - \frac{a^2}{2r_h^2} - \frac{Q^2}{2r_h^2} + \frac{1}{2}(1-b)cr_h^{b-2} - \frac{2\pi r_h}{\tau}, \tag{4.24}$$

$$\phi^{\Theta} = -\cot\Theta\csc\Theta, \tag{4.25}$$

The parameter for the inverse temperature around the Kerr BH in quintessential field can be represented as

$$\tau = \frac{4\pi r_h^3}{-a^2 - Q^2 + r_h^2 + cr_h^b - bcr_h^b}, \tag{4.26}$$

Just like the method used in the previous two sections. The points where the component ϕ^{r_h} equals zero are shown in Fig. 4.7, with $a = 0.1$ and $Q = 1/2$ for different values of $c = 0, 0.1, 0.25$.The unit-magnitude vector field $\mathbf{n}$, with $\tau = 30$, $Q = 1/2$, and $a = 0$, is shown in panel (a) Fig 4.7. These figures help determine the Kerr-Newman solution's topological number in a quintessence field.

$$\omega_1 = 1 \quad \omega_2 = -1 \quad \textit{and} \quad W = 0 \tag{4.27}$$

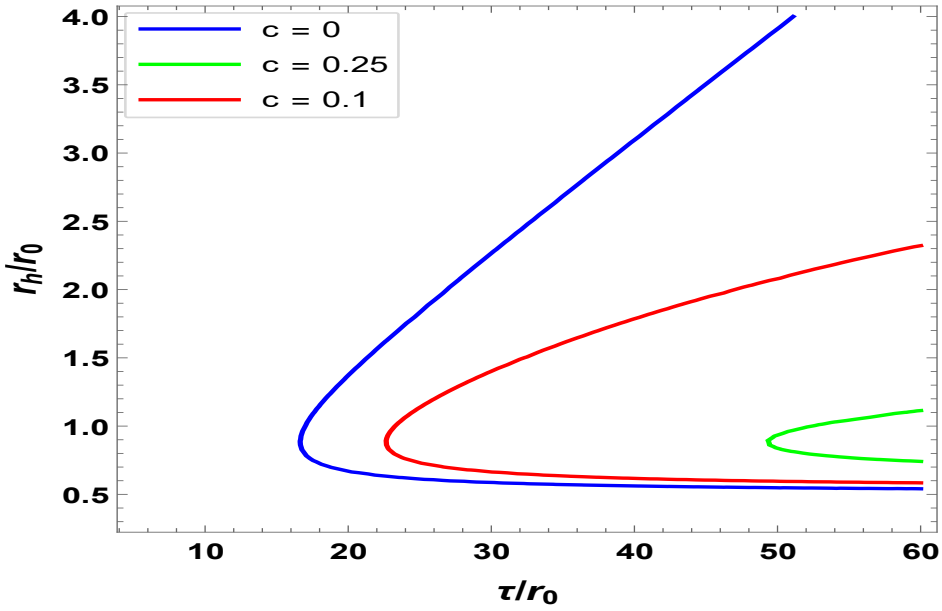

(a) when $\omega = -2/3$ and $a/r_0 = 0.1$. the value τ_c serves as a generation point for different values of c.

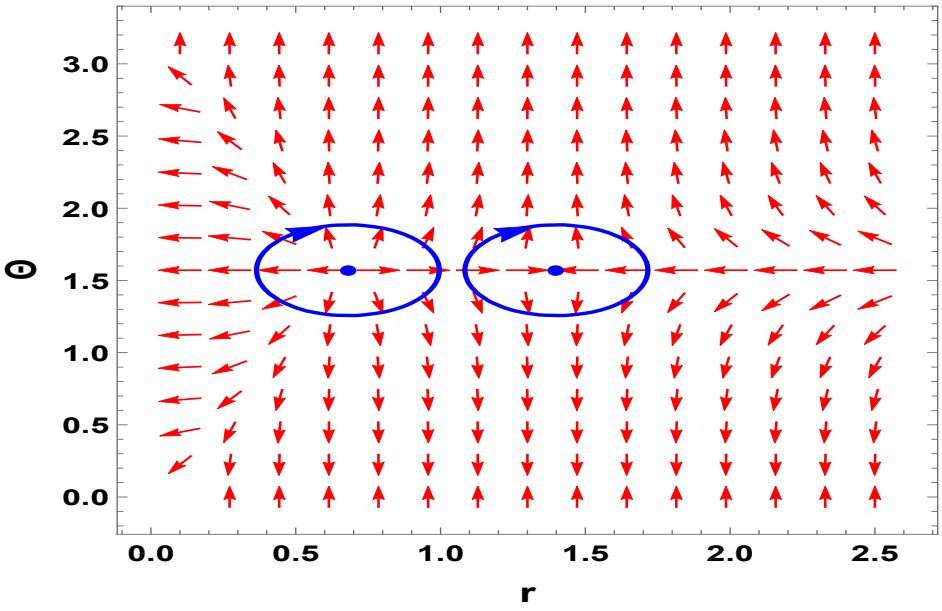

(b) It has been drawn for the Kerr-newman quintessential BH with $a = 0.1$ $\tau/r_0 = 30$ and $c = 0.1$ The zero points ZP_1 and ZP_2 highlighted by blue dots are at $(r_h/r_0, \Theta) = (1.4, \pi/2)$ and $(0.68, \pi/2)$ for ZP_1, and ZP_2 respectively.

Figure 4.7: Graph of rotating Kiselev BH when $\omega = -2/3$

4.4 Kerr-Ads Quintessential BH

We explore how the quintessential field influences the topological classes of Kerr-AdS spacetime. The line element of the Kerr-Ads in a quintessence field is given by [82]

$$ds^2 = \frac{\Sigma}{\Delta_r}dr^2 + \frac{\Sigma}{\Delta_\theta}d\theta^2 + \frac{\Delta_\theta \sin^2\theta}{\Sigma}\left[a\frac{dt}{\Xi} - \left(r^2+a^2\right)\frac{d\phi}{\Xi}\right]^2 - \frac{\Delta_r}{\Sigma}\left(\frac{dt}{\Xi} - a\sin^2\theta\frac{d\phi}{\Xi}\right)^2, \quad (4.28)$$

where

$$\Delta_r = r^2 + a^2 + Q^2 - 2Mr - \frac{\Lambda}{3}r^2\left(r^2+a^2\right) - cr^{1-3\omega}, \quad (4.29)$$

$$\Delta_\theta = 1 + \frac{\Lambda}{3}a^2\cos^2\theta, \quad (4.30)$$

$$\Xi = 1 + \frac{\Lambda}{3}a^2, \quad (4.31)$$

Here,m represents the BHs mass, a its angular momentum per unit mass, c the quintessential parameter, and Λ the cosmological constant. The following expressions describe the mass and other thermodynamic quantities.

$$M = \frac{m}{\Xi}, \quad (4.32)$$

$$S = \frac{\pi\left(r_h^2+a^2\right)}{\Xi}, \quad (4.33)$$

$$T = \frac{r_h^2 - a^2 - Q^2 - \frac{\Lambda}{3}r_h^2\left(3r_h^2+a^2\right) + 3\omega r^{1-3\omega}}{4\pi r_h\left(r_h^2+a^2\right)}, \quad (4.34)$$

For this BH, the off-shell free energy is given by

$$\mathscr{F} = \frac{1}{\Xi}\left[m - \frac{\pi\left(r_h^2+a^2\right)}{\tau}\right], \quad (4.35)$$

This provides components forming the n-vector field can be written as

$$\phi^{r_h} = \frac{1}{\Xi}\left[\frac{1}{2} - \frac{Q^2}{2r_h^2} + \frac{cr_h^{b-2}}{2} - \frac{r_h^2\Lambda}{2} - \frac{a^2(3+r_h^2\Lambda)}{6r_h^2} - \frac{2\pi r_h}{\tau}\right], \quad (4.36)$$

$$\phi^{\Theta} = -\cot\Theta\csc\Theta, \quad (4.37)$$

In the quintessential field, the Kerr-AdS BH's inverse temperature can be simply stated as follows

$$\tau = -\frac{12\pi r_h^3}{3a^2+3Q^2-3r_h^2-3cr_h^b+3bcr_h^b+a^2r_h^2\Lambda+3r_h^4\Lambda}, \tag{4.38}$$

The Kerr-Newman Ads BH, influenced by a quintessence field, exhibits unique topological properties. Its winding numbers are calculated as $\omega_1 = -1$, $\omega_2 = 1$ and $\omega_3 = 1$ which together yield a total topological charge of $W = 1$. These features are visualized in Fig 4.8 Notably, the system includes three distinct critical points both marked as black dots in the Fig 4.9. This interaction between the BH and the quintessence field provides significant insight into the underlying topological framework of the system.

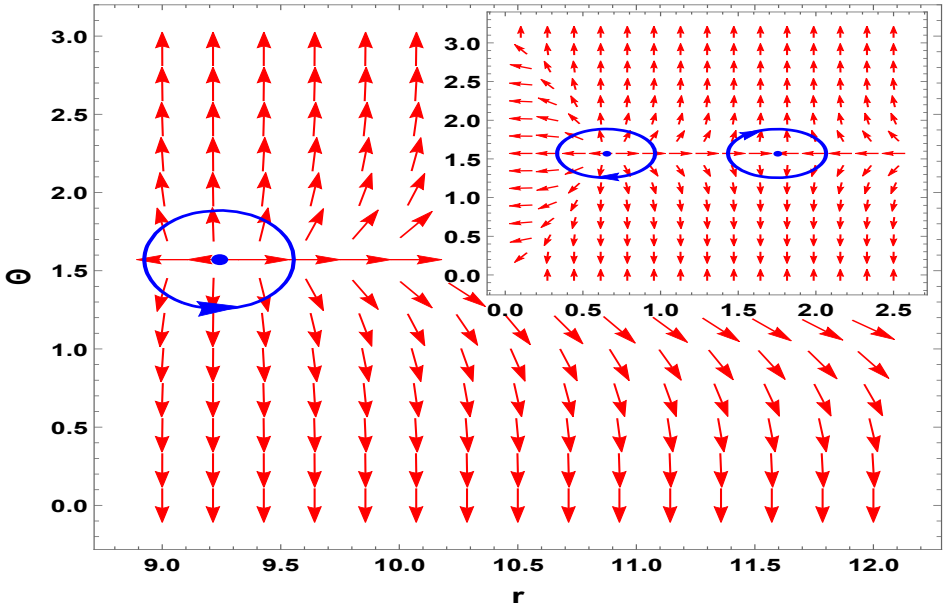

when $\omega = -2/3$, $a/r_0 = 0.1$, $c/r_0 = 0.1$,$\tau/r_0 = 30$ is plotted. Three zero points are located at $(r_h/r_0, \theta)$= $(1.75, \pi/2)$,$(0.65, \pi/2)$, and $(r_h/r_0, \theta)$,= $(9.24, \pi/2)$.

Figure 4.8: Graph of Kerr-Newman Ads BH, when $\omega = -2/3$

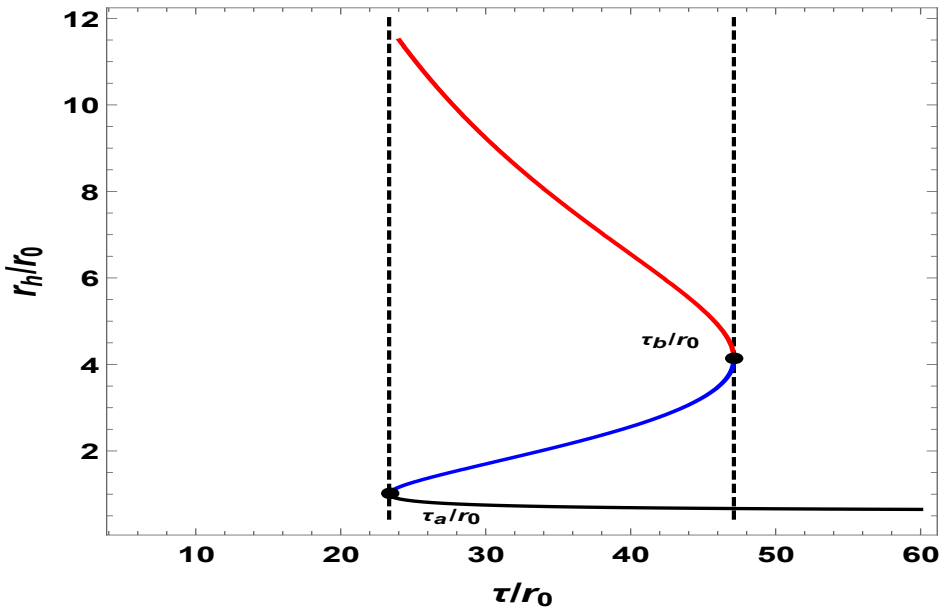

The ZPs of ϕ^{r_h} with $a/r_0 = 0.4$, $\alpha/r_0 = 0.1, \tau/r_0 = 30$ and $Pr_0^2 = 0.0022$ are for Kerr-Ads BH in quintessence field is shown. In the given arrangement, the black, blue, and red solid lines denote the large, intermediate, and small BH. In the case of the Kerr-Ads BH in the quintessence field, a generation point and an annihilation point are present, depicted as black dots.

Figure 4.9: Graph of Kerr-Newman Ads BH, when $\omega = -2/3$

BH Spacetime	**W**	**GP**	**AP**
Kiselev BH	-1	0	0
Rotating Kiselev BH	0	1	0
Kerr-Newman(Quintessential) BH	0	1	0
Kerr-AdS_4(Quintessential) BH	1	1	1 or 0

Table 4.1: Values of W, GP, and AP for different BH spacetimes.

CHAPTER 5

CONTRIBUTION AND FUTURE WORK

5.1 Conclusion

This research has explored the topological classes of stationary axisymmetric black holes and provided valuable insights into their structure and thermodynamic properties. By studying the Kiselev black hole and its rotating version, it was found that the topological number for the Kiselev BH is -1, while the rotating Kiselev BH has a topological number of 0. These results highlight the significant influence of rotation on the fundamental properties of BHs.

To achieve these findings, the research used the relationship between spacetime geometry and thermodynamic quantities such as entropy and temperature. An off-shell free energy function was defined based on the BHs horizon parameter, which allowed for a detailed analysis of the BHs topological behaviors. The study identified critical points that provided insights into the thermodynamic stability and structural features of these BHs. For the rotating Kiselev BH, specific parameter values revealed key behaviors, including the presence of two intersection points at high temperatures. These points demonstrated the relationship between temperature and other parameters, shedding light on the thermodynamic properties of the BH.

One particularly important observation was the behavior of these intersection points under varying conditions. When the parameters reached a critical value, the two points merged and then disappeared, marking a transition in the BHs structure. This critical point acted as a turning point, separating the black hole into two distinct branches. These branches were characterized

by different winding numbers, which ultimately led to the topological number for the rotating Kiselev black hole being identified as zero. This detailed examination underscores the complex interactions between different factors that define black hole thermodynamics and topology.

The findings of this study are significant for understanding black holes on multiple levels. Categorizing black holes into topological classes provides a systematic way to analyze their properties, offering insights into their stability, phase transitions, and thermodynamic behaviors. This framework enhances our understanding of the relationship between black hole structure and thermodynamics, bridging theoretical predictions with practical observations. The topological approach also offers a new perspective for studying the intricate structures of BHs, contributing to the broader understanding of these fascinating cosmic phenomena.

Limitations of the Study

Although this research has provided valuable insights into the topological and thermodynamic behavior of black holes surrounded by quintessence, it is not without limitations. Firstly, the analysis is restricted to specific values of the quintessence parameter and rotation parameters, which may not cover the full dynamical range. Secondly, the study primarily focuses on stationary black hole solutions; therefore, time-dependent or perturbed black hole geometries have not been considered. Finally, the topological methods applied here assume certain symmetries and boundary conditions, which may not hold in more general spacetime configurations.

Future Work

Future investigations may consider extending the analysis to charged black holes or black holes in higher-dimensional spacetimes, potentially revealing new topological behaviors. Additionally, incorporating quantum corrections or modified gravity theories such as $f(R)$ gravity or Gauss-Bonnet gravity could offer deeper insights. Numerical simulations could also be used to explore black hole thermodynamics and topology under varying conditions. Moreover, observational data from gravitational wave detections and black hole imaging (such as from

the Event Horizon Telescope) could help validate the theoretical models presented in this study. These directions of research can further bridge the gap between theory and observation in black hole physics.

BIBLIOGRAPHY

[1] A. Qadir, *Einstein's General Theory of Relativity*. Cambridge Scholars Publishing, 2020.

[2] K. S. Thorne, C. W. Misner, and J. A. Wheeler, *Gravitation*. Freeman San Francisco, 2000.

[3] J. B. Hartle, *Gravity: an Introduction to Einstein's General Relativity*. Cambridge University Press, 2021.

[4] V. Frolov and I. Novikov, *Black Hole Physics: Basic Concepts and New Developments*. Springer Science & Business Media, 2012, vol. 96.

[5] S.-W. Wei, Y.-X. Liu, and R. B. Mann, "Black Hole Solutions as Topological Thermodynamic Defects," *Physical Review Letters*, vol. 129, no. 19, p. 191101, 2022.

[6] M. M. Mansfield and C. O'sullivan, *Understanding Physics*. John Wiley & Sons, 2020.

[7] E. H. TelescopeCollaboration, R. Azulay, A.-K. Baczko, S. Britzen, G. Desvignes, R. Eatough, R. Karuppusamy, J.-Y. Kim, M. Kramer, T. Krichbaum *et al.*, "First M87 Event Horizon Telescope Results. ii. Array and Instrumentation," *apjl*, vol. 875, no. 1, p. L2, 2019.

[8] M. Safronova, D. Budker, D. DeMille, D. F. J. Kimball, A. Derevianko, and C. W. Clark, "Search for New Physics with Atoms and Molecules," *Reviews of Modern Physics*, vol. 90, no. 2, p. 025008, 2018.

[9] L. Smarr, "Surface Geometry of Charged Rotating Black Holes," *Physical Review D*, vol. 7, no. 2, p. 289, 1973.

[10] M. Visser, "The Kerr Spacetime: A Brief Introduction," *arXiv preprint arXiv:0706.0622*, 2007.

[11] K. S. Thorne, "Black Holes and Time Warps," *Einsteins' outrageous Le*, 1982.

[12] S. W. Hawking, “Black Hole Explosions?” *Nature*, vol. 248, no. 5443, pp. 30–31, 1974.

[13] J. M. Bardeen, B. Carter, and S. W. Hawking, “The Four Laws of Black Hole Mechanics,” *Communications in mathematical physics*, vol. 31, pp. 161–170, 1973.

[14] D. N. Page, “Hawking Radiation and Black Hole Thermodynamics,” *New Journal of Physics*, vol. 7, no. 1, p. 203, 2005.

[15] J. D. Bekenstein, “Black Holes and Entropy,” *Physical Review D*, vol. 7, no. 8, p. 2333, 1973.

[16] S. W. Hawking, “Gravitational Radiation from Colliding Black Holes,” *Physical Review Letters*, vol. 26, no. 21, p. 1344, 1971.

[17] A. Strominger and C. Vafa, “Microscopic Origin of the Bekenstein-Hawking Entropy,” *Physics Letters B*, vol. 379, no. 1-4, pp. 99–104, 1996.

[18] R. M. Wald, “The Thermodynamics of Black Holes,” *Living reviews in relativity*, vol. 4, pp. 1–44, 2001.

[19] E. Hubble, “A Relation Between Distance and Radial Velocity Among Extra-Galactic Nebulae,” *Proceedings of the National Academy of Sciences*, vol. 15, no. 3, pp. 168–173, 1929.

[20] E. J. Copeland, M. Sami, and S. Tsujikawa, “Dynamics of Dark Energy,” *International Journal of Modern Physics D*, vol. 15, no. 11, pp. 1753–1935, 2006.

[21] A. G. Riess, A. V. Filippenko, P. Challis, A. Clocchiatti, A. Diercks, P. M. Garnavich, R. L. Gilliland, C. J. Hogan, S. Jha, R. P. Kirshner *et al.*, “Observational Evidence from Supernovae for an Accelerating Universe and a Cosmological Constant,” *The astronomical journal*, vol. 116, no. 3, p. 1009, 1998.

[22] P. M. Garnavich, S. Jha, P. Challis, A. Clocchiatti, A. Diercks, A. V. Filippenko, R. L. Gilliland, C. J. Hogan, R. P. Kirshner, B. Leibundgut *et al.*, “Supernova Limits on the Cosmic Equation of State,” *The Astrophysical Journal*, vol. 509, no. 1, p. 74, 1998.

[23] S. Weinberg, “The Cosmological Constant Problem,” *Reviews of modern physics*, vol. 61, no. 1, p. 1, 1989.

[24] V. Kiselev, "Quintessence and Black Holes," *Classical and Quantum Gravity*, vol. 20, no. 6, p. 1187, 2003.

[25] T. Chiba, T. Okabe, and M. Yamaguchi, "Kinetically Driven Quintessence," *Physical Review D*, vol. 62, no. 2, p. 023511, 2000.

[26] S. Capozziello, "Curvature Quintessence," *International Journal of Modern Physics D*, vol. 11, no. 04, pp. 483–491, 2002.

[27] S. Capozziello, V. F. Cardone, S. Carloni, and A. Troisi, "Curvature Quintessence Matched with Observational Data," *International Journal of Modern Physics D*, vol. 12, no. 10, pp. 1969–1982, 2003.

[28] F. Zwicky, "Die Rotverschiebung von Extragalaktischen Nebeln," *Helvetica Physica Acta, Vol. 6, p. 110-127*, vol. 6, pp. 110–127, 1933.

[29] V. C. Rubin, "Dark Matter in Spiral Galaxies," *Scientific American*, vol. 248, no. 6, pp. 96–109, 1983.

[30] G. Hinshaw, J. Weiland, R. Hill, N. Odegard, D. Larson, C. Bennett, J. Dunkley, B. Gold, M. Greason, N. Jarosik *et al.*, "Five-Year Wilkinson Microwave Anisotropy Probe* Observations: Data Processing, Sky Maps, and Basic Results," *The Astrophysical Journal Supplement Series*, vol. 180, no. 2, p. 225, 2009.

[31] P. A. Ade, N. Aghanim, M. Arnaud, M. Ashdown, J. Aumont, C. Baccigalupi, A. Banday, R. Barreiro, J. Bartlett, N. Bartolo *et al.*, "Planck 2015 Results-XIII. Cosmological Parameters," *Astronomy & Astrophysics*, vol. 594, p. A13, 2016.

[32] S. Schaffer, "John Michell and Black Holes," *Journal for the History of Astronomy, Vol. 10, P. 42, 1979*, vol. 10, p. 42, 1979.

[33] E. M. Slayter and H. S. Slayter, *Light and Electron Microscopy*. Cambridge University Press, 1992.

[34] C. Montgomery, W. Orchiston, and I. Whittingham, "Michell, Laplace and the Origin of the Black Hole Concept," *Journal of Astronomical History and Heritage*, vol. 12, pp. 90–96, 2009.

[35] C. C. Gillespie and R. Thiele, "Pierre-Simon Laplace, 1749-1827. a Life in Exact Science," *Annals of Science*, vol. 56, no. 3, 1999.

[36] A. Hamilton, "Journey into a Schwarzschild Black Hole, Jila: A Joint Institute of Nist and the University of Colorado Boulder," 2020.

[37] B. Schutz, *Gravity from the Ground up: An Introductory Guide to Gravity and General Relativity*. Cambridge university press, 2003.

[38] A. Loinger, "Revisiting the Einstein Field of a Mass Point," *Arxiv preprint gr-qc/9908009*, 1999.

[39] J. Droste, "The Field of a Single Centre in Einstein's Theory of Gravitation, and the Motion of a Particle in that Field," *Ned. Acad. Wet., SA*, vol. 19, p. 197, 1917.

[40] A. J. Kox, "General Relativity in the Netherlands, 1915–1920," *Eisenstaedt and Kox*, pp. 39–56, 1992.

[41] A. S. Eddington, *The Internal Constitution of the Stars*. Cambridge University Press, 1988.

[42] G. Venkataraman, *Chandrasekhar and his Limit*. Universities Press, 1992.

[43] E. Gallo and D. Marolf, "Resource Letter Bh-2: Black Holes," *American Journal of Physics*, vol. 77, no. 4, pp. 294–307, 2009.

[44] P. Jekel and E. Witten, "Life in the Extreme."

[45] J. R. Oppenheimer and G. M. Volkoff, "On Massive Neutron Cores," *Physical Review*, vol. 55, no. 4, p. 374, 1939.

[46] B. Margalit and B. D. Metzger, "Constraining the Maximum Mass of Neutron Stars from Multi-Messenger Observations of Gw170817," *The Astrophysical Journal Letters*, vol. 850, no. 2, p. L19, 2017.

[47] R. Ruffini and J. A. Wheeler, "Introducing the Black Hole," *Physics today*, vol. 24, no. 1, pp. 30–41, 1971.

[48] J. Bernstein, "The Reluctant Father of Black Holes," *Scientific American*, vol. 274, no. 6, pp. 80–85, 1996.

[49] J. R. Oppenheimer and H. Snyder, "On Continued Gravitational Contraction," *Physical Review*, vol. 56, no. 5, p. 455, 1939.

[50] D. Finkelstein, "Past-Future Asymmetry of the Gravitational Field of a Point Particle," *Physical Review*, vol. 110, no. 4, p. 965, 1958.

[51] M. D. Kruskal, "Maximal Extension of Schwarzschild Metric," *Physical review*, vol. 119, no. 5, p. 1743, 1960.

[52] A. Hewish, S. J. Bell, J. D. Pilkington, P. Frederick Scott, and R. A. Collins, "Observation of a Rapidly Pulsating Radio Source," in *A Source Book in Astronomy and Astrophysics, 1900–1975*. Harvard University Press, 1979, pp. 498–504.

[53] J. Pilkington, A. Hewish, S. Bell, and T. Cole, "Observations of some Further Pulsed Radio Sources," *Nature*, vol. 218, no. 5137, pp. 126–129, 1968.

[54] K. Kotera and A. V. Olinto, "The Astrophysics of Ultrahigh-Energy Cosmic Rays," *Annual Review of Astronomy and Astrophysics*, vol. 49, no. 1, pp. 119–153, 2011.

[55] E. T. Newman, E. Couch, K. Chinnapared, A. Exton, A. Prakash, and R. Torrence, "Metric of a Rotating, Charged Mass," *Journal of mathematical physics*, vol. 6, no. 6, pp. 918–919, 1965.

[56] W. Israel, "Event Horizons in Static Vacuum Space-Times," *Physical review*, vol. 164, no. 5, p. 1776, 1967.

[57] B. Carter, "Axisymmetric Black Hole has only Two Degrees of Freedom," *Physical Review Letters*, vol. 26, no. 6, p. 331, 1971.

[58] D. C. Robinson, "Uniqueness of the Kerr Black Hole," *Physical Review Letters*, vol. 34, no. 14, p. 905, 1975.

[59] P. T. Chruściel, J. L. Costa, and M. Heusler, "Stationary Black Holes: Uniqueness and Beyond," *Living Reviews in Relativity*, vol. 15, pp. 1–73, 2012.

[60] R. Penrose, "Gravitational Collapse and Space-Time Singularities," *Physical Review Letters*, vol. 14, no. 3, p. 57, 1965.

[61] L. H. Ford, "The Classical Singularity Theorems and their Quantum Loopholes," *International Journal of Theoretical Physics*, vol. 42, pp. 1219–1227, 2003.

[62] R. Penrose, R. Genzel, and A. Ghez, "The Nobel Prize in Physics 2020," 2020.

[63] H. Shipman, "The Implausible History of Triple Star Models for Cygnus x-1 Evidence for a Black Hole," *Astrophysical Letters, vol. 16, no. 1, 1975, p. 9-12. Research supported by the Research Corp.*, vol. 16, pp. 9–12, 1975.

[64] B. P. Abbott, R. Abbott, T. Abbott, M. Abernathy, F. Acernese, K. Ackley, C. Adams, T. Adams, P. Addesso, R. X. Adhikari *et al.*, "Observation of Gravitational Waves from a Binary Black Hole Merger," *Physical review letters*, vol. 116, no. 6, p. 061102, 2016.

[65] E. H. T. Collaboration *et al.*, "First m87 Event Horizon Telescope Results. I. the Shadow of the Supermassive Black Hole," *arXiv preprint arXiv:1906.11238*, 2019.

[66] S. Gillessen, F. Eisenhauer, S. Trippe, T. Alexander, R. Genzel, F. Martins, and T. Ott, "Monitoring Stellar Orbits around the Massive Black Hole in the Galactic Center," *The Astrophysical Journal*, vol. 692, no. 2, p. 1075, 2009.

[67] H. C. L. Junior, J.-Z. Yang, L. C. Crispino, P. V. Cunha, and C. A. Herdeiro, "Einstein-maxwell-dilaton Neutral Black Holes in Strong Magnetic Fields: Topological Charge, Shadows, and Lensing," *Physical Review D*, vol. 105, no. 6, p. 064070, 2022.

[68] R. P. Kerr, "Gravitational Field of a Spinning Mass as an Example of Algebraically Special Metrics," *Physical review letters*, vol. 11, no. 5, p. 237, 1963.

[69] R. C. Myers and M. J. Perry, "Black Holes in Higher Dimensional Space-Times," *Annals of Physics*, vol. 172, no. 2, pp. 304–347, 1986.

[70] S.-W. Wei, P. Cheng, and Y.-X. Liu, "Analytical and Exact Critical Phenomena of d-Dimensional Singly Spinning Kerr-AdS Black Holes," *Physical Review D*, vol. 93, no. 8, p. 084015, 2016.

[71] E. T. Newman and A. Janis, "Note on the Kerr Spinning-Particle Metric," *Journal of Mathematical Physics*, vol. 6, no. 6, pp. 915–917, 1965.

[72] E. T. Newman, E. Couch, K. Chinnapared, A. Exton, A. Prakash, and R. Torrence, "Metric of a Rotating, Charged Mass," *Journal of mathematical physics*, vol. 6, no. 6, pp. 918–919, 1965.

[73] Z. Xu, X. Hou, and J. Wang, "Kerr–anti-de Sitter/de Sitter Black Hole in Perfect Fluid Dark Matter Background," *Classical and Quantum Gravity*, vol. 35, no. 11, p. 115003, 2018.

[74] S. H. Hendi, A. Nemati, K. Lin, and M. Jamil, "Instability and Phase Transitions of a Rotating Black Hole in the Presence of Perfect Fluid Dark Matter," *The European Physical Journal C*, vol. 80, pp. 1–12, 2020.

[75] C. Fang, J. Jiang, and M. Zhang, "Revisiting Thermodynamic Topologies of Black Holes," *Journal of High Energy Physics*, vol. 2023, no. 1, pp. 1–17, 2023.

[76] D. Wu *et al.*, "Topological Classes of Rotating Black Holes," *Physical Review D*, vol. 107, no. 2, p. 024024, 2023.

[77] K. Jusufi, M. Jamil, and M. Rizwan, "On the Possibility of Wormhole Formation in the Galactic Halo due to Dark Matter Bose–Einstein Condensates," *General Relativity and Gravitation*, vol. 51, no. 8, p. 102, 2019.

[78] A. Das, A. Saha, and S. Gangopadhyay, "Investigation of Circular Geodesics in a Rotating Charged Black Hole in the Presence of Perfect Fluid Dark Matter," *Classical and Quantum Gravity*, vol. 38, no. 6, p. 065015, 2021.

[79] T.-C. Ma, H.-X. Zhang, P.-Z. He, H.-R. Zhang, Y. Chen, and J.-B. Deng, "Shadow cast by a Rotating and Nonlinear Magnetic-Charged Black Hole in Perfect Fluid Dark Matter," *Modern Physics Letters A*, vol. 36, no. 17, p. 2150112, 2021.

[80] B. Toshmatov, Z. Stuchlík, and B. Ahmedov, "Rotating Black Hole Solutions with Quintessential Energy," *The European Physical Journal Plus*, vol. 132, pp. 1–21, 2017.

[81] M. Rizwan and K. Jusufi, "Topological Classes of Thermodynamics of Black Holes in Perfect Fluid Dark Matter Background," *The European Physical Journal C*, vol. 83, no. 10, p. 944, 2023.

[82] J. Toledo and V. Bezerra, "Kerr–Newman–Ads Black Hole with Quintessence and Cloud of Strings," *General Relativity and Gravitation*, vol. 52, pp. 1–21, 2020.